INFLUENCE OF INDUCED UNBALANCE ON SUBSYNCHRONOUS VIBRATIONS OF AN AUTOMOTIVE TURBOCHARGER

John Sterling

Thesis submitted to the faculty of the Virginia Polytechnic Institute and State University in partial fulfillment of the requirements for the degree of

MASTER OF SCIENCE

in

MECHANICAL ENGINEERING

Dr. R. Gordon Kirk, Chairman

Dr. Mary E. Kasarda, Member

Dr. Alfred Wicks, Member

June 22, 2009

Blacksburg, Virginia

Keywords: Turbocharger, Instability, Subsynchronous, Unbalance

INFLUENCE OF INDUCED UNBALANCE ON SUBSYNCHRONOUS VIBRATIONS OF AN AUTOMOTIVE TURBOCHARGER

John Sterling

ABSTRACT

Rotordynamic instability is present in most or all automotive turbochargers. High subsynchronous amplitudes can cause a variety of problems in areas such as mechanical failures, emissions regulations and rotor design. Self-excited vibrations from sources of damping can lock in at lateral natural frequencies causing dangerously high vibration levels. The resulting high-amplitude conical and bending modes can be reduced in order to achieve a more robust system.

This research focuses on the relationship between synchronous and subsynchronous amplitude levels. It is theorized that an increase in unbalance could cause a reduction in subsynchronous vibration amplitudes. Through the use of a custom turbocharger, a series of unbalances were applied to both the turbine and compressor wheels and the resulting amplitudes were recorded off a modified compressor nut. The resulting data were reduced and are presented at the end of this paper.

ACKNOWLEDMENTS

My greatest thanks go out to Dr. Kirk for allowing me a chance to continue my academic career with a Master of Science. It has made an important difference in my life and thanks to him, I have progressed much, both academically and professionally. I would like to thank Dr. Kasarda and Dr. Wicks for some invaluable advice and guidance at times when it was needed most.

I would also like to thank all the members of the Rotordynamics Industry Affiliates group for all of their donations, and especially Allan Kelly and Paul Diemer at Borg-Warner Turbosystems. Without their continued support and guidance, this research would not have been possible. I would also like to personally thank Dan Petersen for introducing me to the Linearity Core, which became the first revision of the experimental hardware.

Lastly, I would like to thank my mother for constant, unwavering support from a distance, and Ashley Ailsworth for personal support and assistance throughout this research.

TABLE OF CONTENTS

LIST OF FIGURES

LIST OF TABLES

NOMENCLATURE

Symbol	Description	Units
mils	“milli-inch”	1/1000 inch
N	Shaft Rotational Velocity	RPM
Subsync	Subsynchronous Vibration	---
Sync	Synchronous Vibration	---
Uc	Induced Compressor Unbalance.	g*mm
Ut	Induced Turbine Unbalance.	g*mm

CHAPTER 1

Introduction and Literature Review

1.1 Introduction

Turbochargers are a class of turbomachinery intended to increase the power of internal combustion engines. This is accomplished by increasing the pressure of intake air, allowing more fuel to be combusted. In the late 19th century, Rudolf Diesel and Gottlieb Daimler experimented with pre-compressing air to increase the power output and fuel efficiency. The first exhaust gas turbocharger was completed in 1925 by the Swiss engineer Alfred Buchi who introduced a prototype to increase the power of a diesel engine by a reported 40%. The idea of turbocharging at that time was not widely accepted. However, in the last few decades, it has become essential in almost all diesel engines with the exception of very small diesel engines [1]. Their limited use in gasoline engines has also resulted in a substantial boost in power output and efficiency. Their total design, as in other turbomachines, involves several analyses including: mechanical, aerodynamic, thermal, and acoustic. Engineers and researchers still seek ways to improve their designs while governed by rules of cost and manufacturing capabilities.

At first, scientists simply attempted to develop the conceptual designs into reliable products for end users. These turbochargers were very large and were mostly destined for marine applications. Because of this, their studies were based on the output performance of the turbochargers with focus on the thermodynamics of the process. Although rotordynamic analysis is now an important part of the design process, a thorough rotordynamic investigation was then very difficult and relatively few studies were published.

By 1938, the first turbocharged automobile engine was manufactured by “Swiss Machine Works Saurer”. Turbocharged automobiles were plagued by reliability issues and with some spectacular failures like the Chevrolet Corvair (last made in 1963), turbocharged engines had essentially been removed from the market.

Turbocharged engines made a comeback during the oil shortage in the early 70’s due to their inherent increase in fuel efficiency. Then, starting in the late 80’s, the beginning of ever-tightening EPA restrictions made it so that the vast majority of diesel engines were and are still turbocharged.

The advances in rotordynamic analysis using up-to-date computation technology have made the dynamics of a turbocharger’s rotor-bearing system a rich area for investigation. Vendors are now looking for more dynamically stable turbochargers to benefit business and increase customer satisfaction. More contributions are needed to have optimum design stability, while assuring continued low cost production.

They also require a high level of reliability and efficiency in order to be cost-effective. There are several ways to reduce the price of turbochargers; the easiest way is to keep the design as simple as possible. A common design assembly in an automotive turbocharger consists of a simple inboard bearing mounting arrangement with a radial outflow compressor and a radial inflow turbine on a single shaft. Figure 1.1 below shows a cut-away view of a common automotive turbocharger.

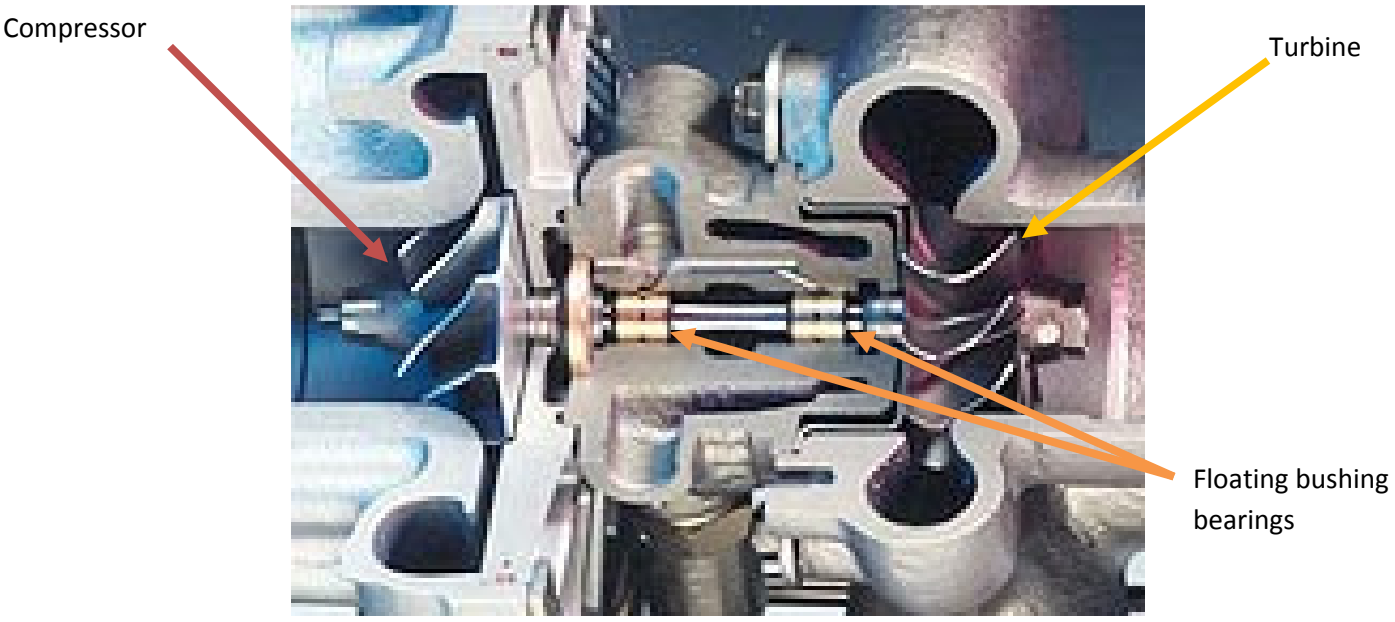

Figure 1.1 Turbocharger cut-away view

This research focuses on the difference between the unbalance vibration and subsynchronous (destabilizing) vibration in the rotor. The experiment aims to evaluate the dynamic stability of an automotive turbocharger rotor-bearing system through a wide range of unbalance levels. The development of a diesel engine test stand and the associated data acquisition system will be discussed, followed by the presentation of a portion of the data reduced to date.

1.2 Literature review

The most important factor in the design of an automotive turbocharger is the initial cost. Engineers aim to cut the cost of producing larger engines capable of providing the same power. Even though truck engines operate at modest break-mean-effective-pressure (~14 bar) and hence at lower boost pressure (up to 2.5:1), they work at an extremely high exhaust temperature [1]. Because truck engines are used in heavy operations, they demand good acceleration and high torque over a wide speed range.

The compressor impeller in most automotive turbochargers is made of aluminum (LM-16-WP or C-355T61). Aluminum LM-27-M is also used for the compressor casing, unless the compressor impeller is made from material other than aluminum. The turbine rotor needs to withstand high operating temperatures that could be as high as 1000 K (1340.6 °F), or more, and also withstand high operating pressures. The most convenient material to use for that purpose is 713C Inconel, a high nickel alloy. The turbine rotor casing should also withstand high temperatures, but does not need to resist the high pressures that the turbine rotor experiences. There are three different types of materials used for the turbine rotor casing depending on their operating temperatures. S.G. iron (spheroidal graphite) is used for operating temperatures up to 975 K, high-silicon S.G. iron is for temperatures up to 1000 K, and high nickel cast iron for temperatures above 1000 K. The shaft is usually made of high-carbon steel (C1144 steel, EN 19C) to allow induction hardening of the journals. The turbine rotor in most common automotive turbochargers is connected to its shaft by using friction welding or an electron beam welding method. The compressor wheel, or impeller, is usually a very light interference fit on the other end of the shaft. A self locking nut is used to hold the impeller against an abutment on the shaft. The friction that is created by the nut is able to keep the entire rotating assembly in place, and is a highly studied joint in industry even now. Due to this, no gear splines or keyways are needed. Figures 1.2 and 1.3 show the basic rotordynamic elements of a typical automotive turbocharger.

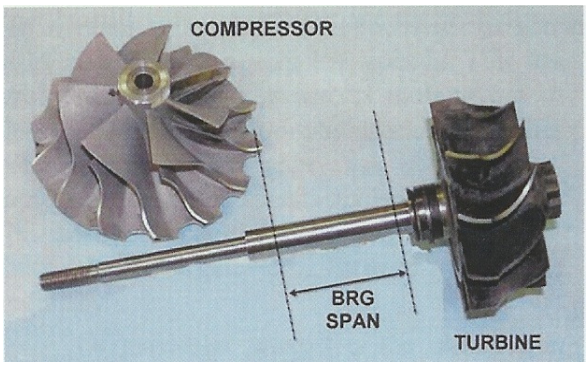

Figure 1.2 Disassembled turbocharger [2]

Figure 1.3 Floating ring bearings [2]

Most automotive-size turbochargers incorporate journal or floating bushing bearings. These bearings are designed to reduce the friction losses that would occur with a fixed lobe or journal bearing. Turbochargers use the engine oil system in lubricating their bearings for low cost and simplicity of maintenance instead of having a separate system. Ball bearings are not used for most commercial engine applications because of their short life and their difficult access for replacement. Special high performance engines in automotive racing applications can afford the added expense of ball bearings, and cutting-edge designs make use of ceramic ball elements.

One of the primary considerations in the design of high-speed rotating machinery with regard to rotordynamics is to control and minimize the response of forced vibration, rotor unbalance in particular. But there exists another class of vibration, termed rotordynamic instability and self excited vibration, which involves an additional set of design approaches, requirements, and constraints to ensure trouble-free, quiet, and durable rotating machinery [4].

Almost all rotors of automotive turbochargers exhibit strong subsynchronous vibrations, as well as the more common unbalance vibrations found in other rotating machinery. These vibrations are undesirable because they generate noise, and can have large amplitudes that cause

rotor-stator rub [5]. Unbalance vibrations are harmonic, or synchronous, with shaft speed and generally arise from two main causes: mass eccentricity and shaft bow. Mass eccentricity is a natural phenomenon in all rotors due to the offset of mass centroid, and shaft bow is commonly caused by thermal effects.

Self-excited vibrations, on the other hand, are different from the forced or unbalance vibrations. They often develop during the operation of the rotor, but they do not naturally exist there. In other words, when the rotor stops running, the mechanical unbalance will still exist, but the sources of self-excited vibrations will not. Rotordynamic instabilities that are caused by self-excited lateral vibrations occur at the system's natural frequencies, which are subsynchronous, meaning below the running speed. These instabilities usually increase as the running speed increases, until nonlinearities in the system limit higher amplitudes. The mechanisms of self-excitation are categorized as: whipping and whirling, parametric instabilities, stick-slip rubs and chatter, and instabilities in forced vibrations [4]. Subsynchronous instabilities in turbochargers are commonly referred to as whirling or whipping. Whirling and whipping can arise as the viscous fluid circulates in the bearing clearance with an average velocity of about one-half the shaft's surface speed. In a whirling phenomenon, the vibration will be at some percentage of the shaft speed. In whipping, the vibration frequency locks in at a single frequency and remains there as the shaft speed increases. The main sources of whirling and whipping in turbochargers are: internal rotor damping (hysteretic whirl), fluid-film journal bearings, and aerodynamic cross-coupling. The research in this document highlights the effects that unbalance has on the rotordynamic instability in turbochargers.

Instabilities are problematic in business because of the operational delays they cause, in terms of delayed certification and release. This delay is also prelude to redesign and modification costs. These factors supply the need to design a stable turbocharger rotor bearing system, which

becomes a top priority for manufacturers. In the past, there were not many research works presented for the rotordynamics of turbochargers because of a shortage of alternative and inexpensive methods of examining model design [5, 6, 7]. In recent years, developments in computational methods have made the design process much easier, faster, and reliable [2, 3, 8-12]. There are many approaches to improve the stability in automotive turbochargers, one of which is to modify the bearing characteristics. Bearing type, bearing shape, and bearing preloads can also be modified. Most automotive turbocharger bearing systems use floating ring bushing bearings like the bearings shown in Figure 1.2. These bearings have the most favorable relationship of reliable, stable operation to manufacturing cost currently available in the market. However, most recent research [2, 5, 9] shows that subsynchronous vibrations still exist in these floating ring bearings with high amplitudes. With the use of advanced computational methods, evaluation of turbocharger rotordynamics becomes a vital part of the design process. Previous experimental work on the vibration of a typical turbocharger with floating ring bearings was presented by Holmes [5]. Figure 1.3 clearly shows the high subsynchronous vibrations amplitudes found in that turbocharger. This spectrum content shows that the lower sub-synchronous whirl instability starts at very low speeds, and dominates over a large speed range. The low frequency whirl mode is a rigid body mode of conical shape, where the turbine and compressor wheels are moving out of phase. Below 40,000 RPM, mixed mode action is visible with both conical and bending modes at work. At speeds above 40,000 RPM, the second whirl mode is the dominant mode.

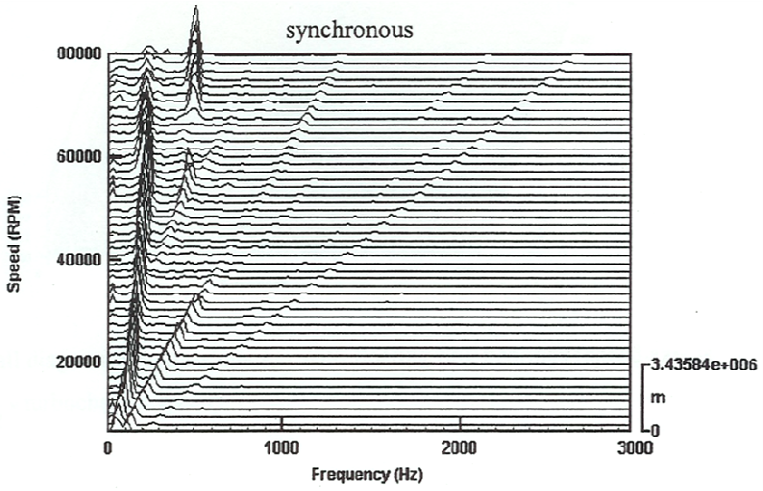

Figure 1.4 Turbocharger waterfall plot

Additional recent experimental work has been reported on a research turbocharger configuration which reveals interesting details of the total turbo shaft and bearing system dynamics but from a bench test configuration [13].

This research aims to show experimentally that the addition of unbalance can suppress the appearance and magnitude of subsynchronous vibrations. Results of this type have not yet been published publicly. This phenomenon is shown to exist analytically by Kirk [18,19] and numerically by Chen and Gunter [3].

Chapter 2

Test Stand and Procedure

2.1 Test Stand and Data Acquisition

The test stand in the Mechanical Engineering IC Engine Lab has a unique suite of sensors coupled with a diesel engine test platform. The purpose of this test stand has specifically been to measure the vibration of turbochargers, and several different types and sizes have been studied. This system has existed in the Virginia Tech Mechanical Engineering facilities for four years, and the DAQ system has seen myriad tests with good results using the OEM turbocharger [15-17]. It took both custom components and stock engine components to install the engine on the dynamometer test stand in the Mechanical Engineering IC Engine Laboratory shown in Figure 2.1. It was necessary to install the engine mounts, the drive coupling adaptor plate, the oil feed and drain lines, the electrical wiring for the starter and fuel pump, the coolant feed and drain lines, and the exhaust lines. An optical speed sensor and two orthogonal displacement probes were added to the turbocharger, as shown in Figure 2.2. Velocity sensors are used to monitor the engine block vibration.

The use of available instrumentation was attempted but special equipment from Bently-Nevada was necessary to monitor such high frequency and small diameter shafting. Two non-contacting, inductive proximity probes were used to measure the vibration of the turbocharger, and the signal had to go through significant conditioning thereafter. The instrumentation cart used for the project is shown in Figure 2.3 and further described in Table 2.1. Figure 2.4 shows the digital readout used to track real-time RPM.

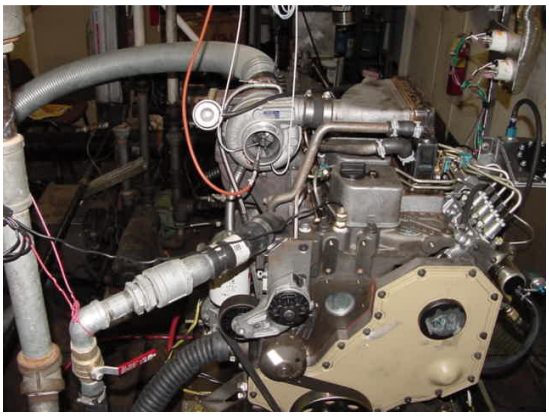

Figure 2.1. Diesel engine on test stand at Virginia Tech

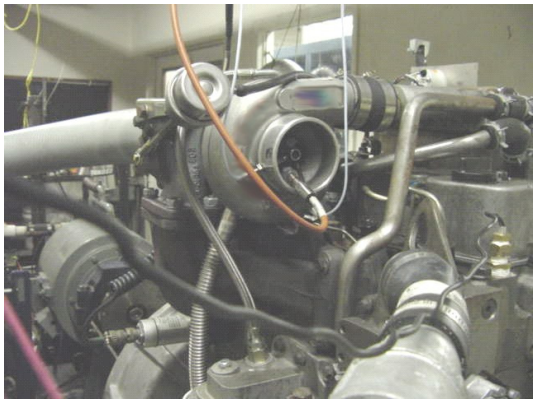

Figure 2.2. Compressor inlet with optical speed Sensor

Figure 2.3. Data acquisition system

Table 2.1 Current test stand instrumentation

2 - 8 ch PC based data acquisition

2 – amplitude, phase and speed vector filters

2 - x-y Oscilloscopes

1 - 400 line FFT Analyzer

2 – velocity seismic probes

1 – Keyphasor conditioner

2 – power supplies

4 - non-contact shaft probes

2 – normal probe drivers

2 – special probe drivers

2 – optical speed sensors

1 – boost pressure gage

1 – temperature gage

1 – engine dyno

Figure 2.4. Bently-Nevada Digital Vector Filter

Because an optical sensor is being used, its performance is based on receiving a reflection from a blade on the compressor wheel. Due to the high speed of the compressor, getting a proper reflection from the keyphasor blade has been a concern from the beginning. Keyphasor signal integrity and the associated lighting solutions have been changing and upgrading over the four year duration of the project. In order to increase its viability as a target, the keyphasor blade is painted white with reflective paint, and the other blades marked black. This ensures that there will be one and only one voltage peak per cycle. Several lighting iterations have existed, including fluorescent, LED, and halogen sources, in various mounting fixtures. The current evolution uses an incandescent flashlight with a focusing lens mounted on a microphone stand and is shown in Figures 2.5 and 2.6. The microphone stand has two lockable points of articulation and the flashlight has an adjustable focus. This combination has allowed for excellent signal quality of the optical transducer. A picture of the current system is shown in Figure 2.7. To date, this has produced a strong signal up to 90krpm with excellent reliability.

Figure 2.5. Light source stand

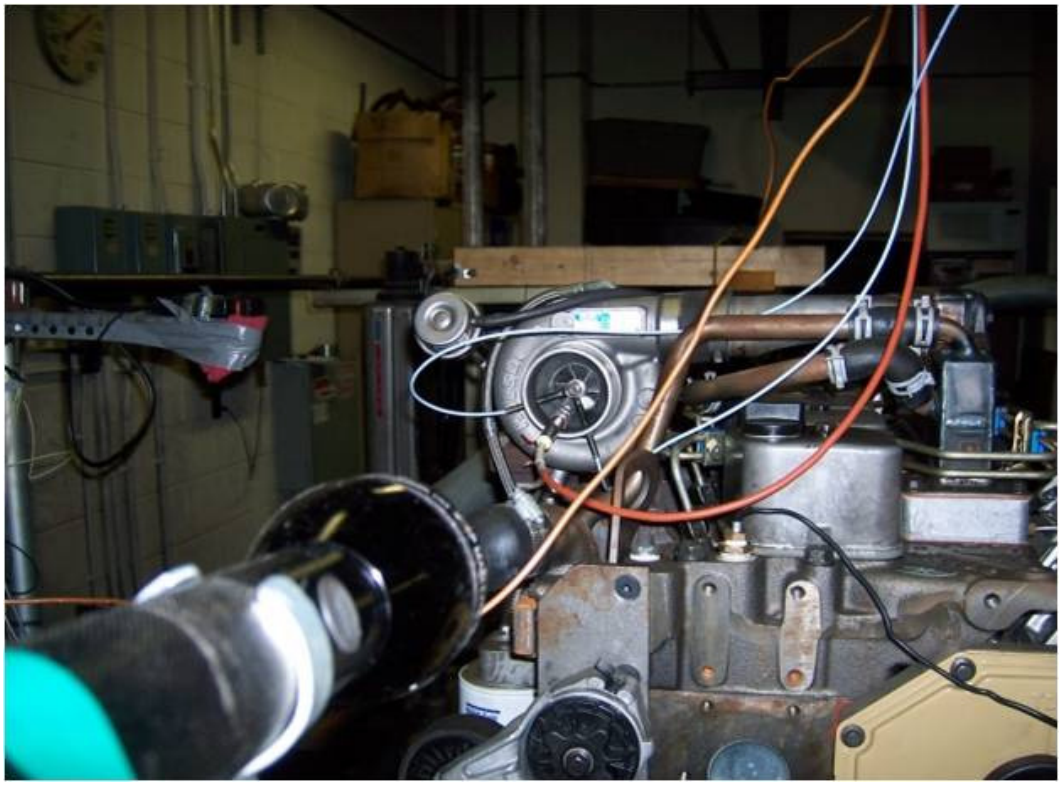

Figure 2.6. Flashlight view of the turbo.

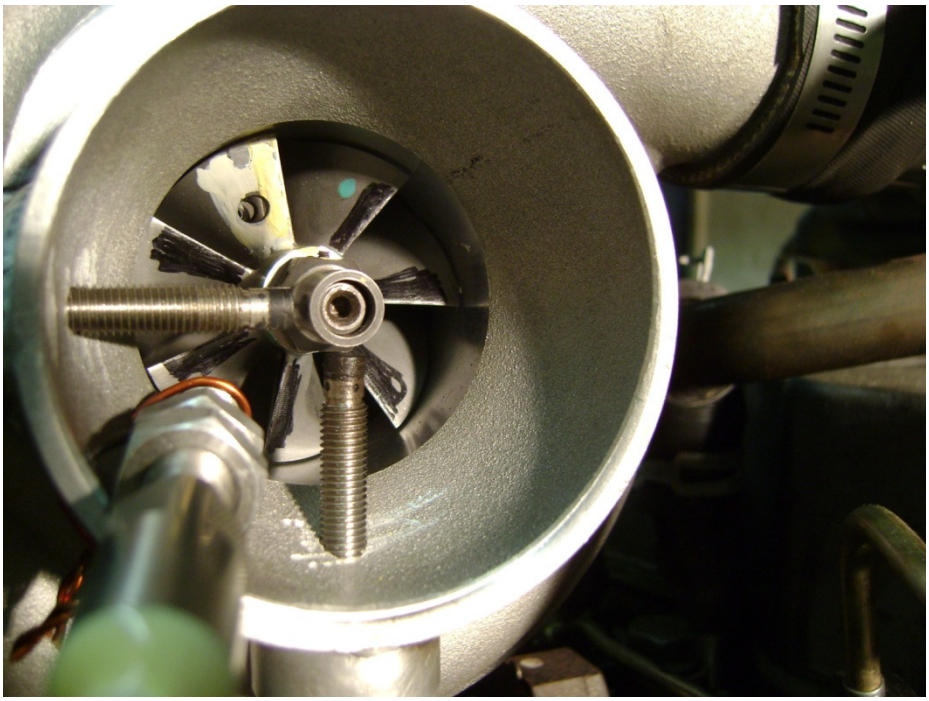

Figure 2.7. Closeup of the transducers and the keyphasor blade.

A basic “dashboard” was created to show some vital engine data: boost, coolant temperature, and oil pressure. Gauges with peak/hold function were used to assure consistent engine conditions from run to run. Figure 2.8 below is a picture of the dashboard.

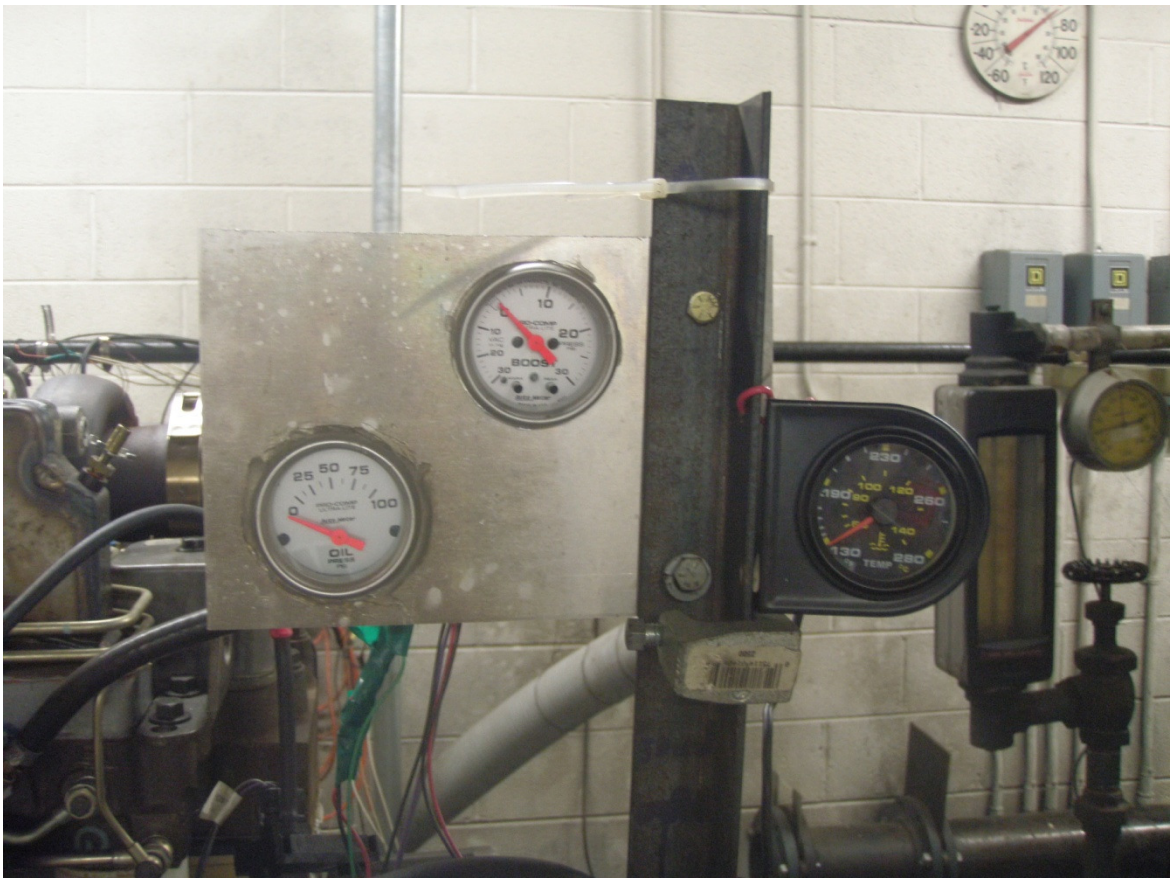

Figure 2.8. The dashboard.

2.2 Test Turbocharger

In this research, a custom turbocharger was matched to the engine and assembled with a 70 mm compressor mated to a 70 mm turbine. Some particularly difficult machining was accomplished on both of the wheels using wire EDM. In this configuration, a pair of threaded holes is applied to the deck of either the compressor or turbine, 180 degrees out of phase. This

allows imbalancing mass in the form of M5 set screws to be inserted. Stock lengths of 1/8", 3/16", and 1/4" were obtained and could be filed down manually to create specifically desired weights. As designed, the unbalance on the rotor can be changed quickly and without having to disassemble the unit. This is ideal from a repeatability standpoint. Figures 2.11 and 2.12 show some significant dimensions and prints of the wheels are included in the appendix.

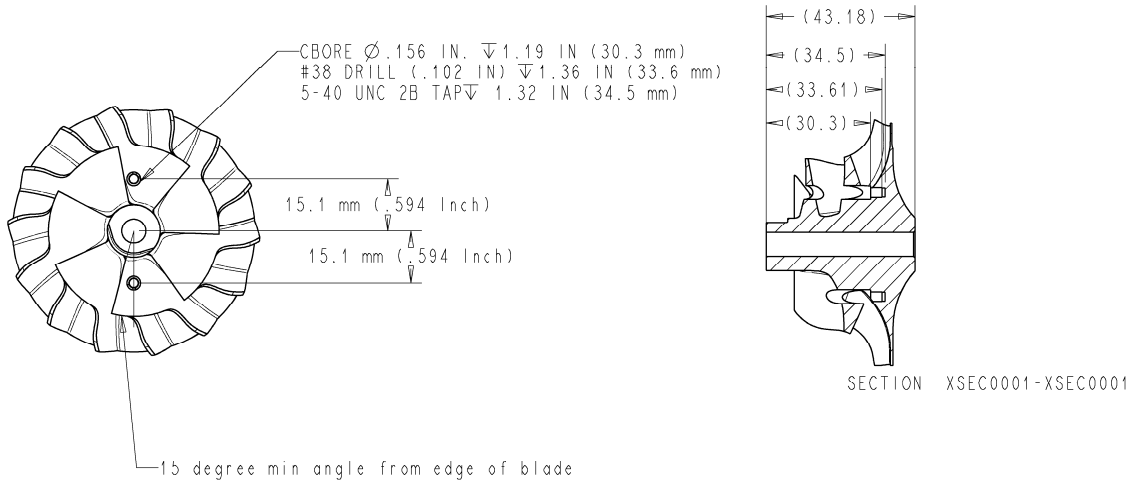

Figure 2.11. Dimensioned drawing of compressor

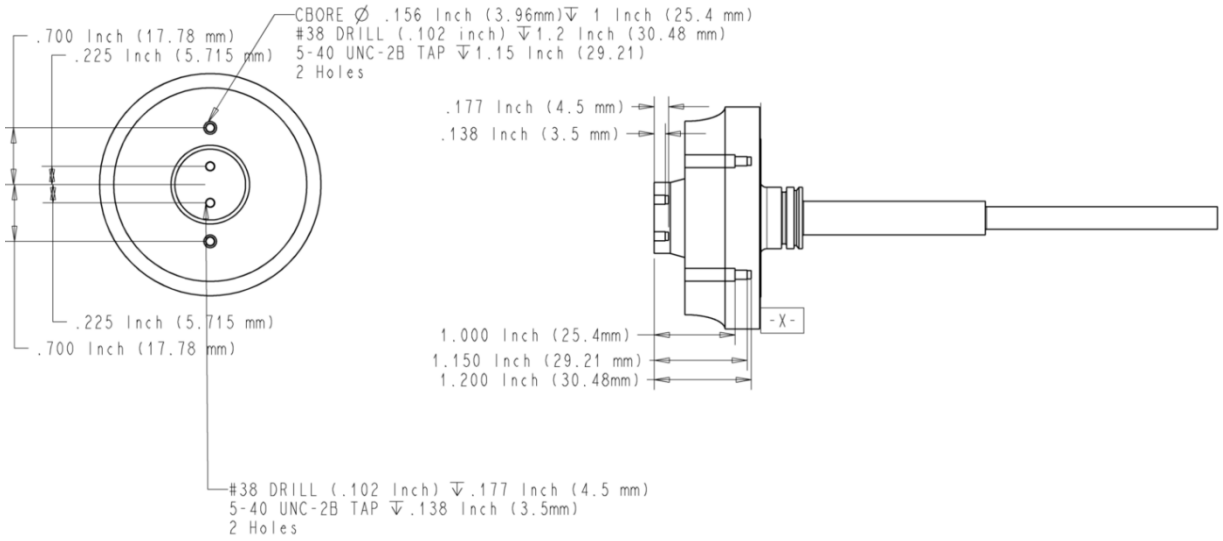

Figure 2.12. Dimensioned drawing of turbine

Two counterbored threads were machined into the compressor at a radius of 15.1 mm. Four counterbored threads are in the turbine: two in the deck at 17.78 mm and two in the shaft at 5.715 mm. This is done to allow for the possibility of adding extra unbalance to achieve a desired effect, or for finer unbalance control, but was not used for this experiment. The unbalance is then calculated as the product of the distance and mass.

On the compressor end, a special lock nut with an extended tip is used. Sometimes called a "target nut", this tip makes the use of proximity sensors much simpler. It is approximately four times longer than a standard lock nut, and the extra length is made up of circular extruded section to allow sensors to have a regular surface to monitor. Also visible is a small balance weight used for extremely fine tuning of rotor balance. This was not changed during the course of the experiment, nor was it necessary to remove the target nut. Visible is the extended target area for the proximity probes. Figure 2.13 shows a close-up of the target nut. This nut is visible in several other pictures.

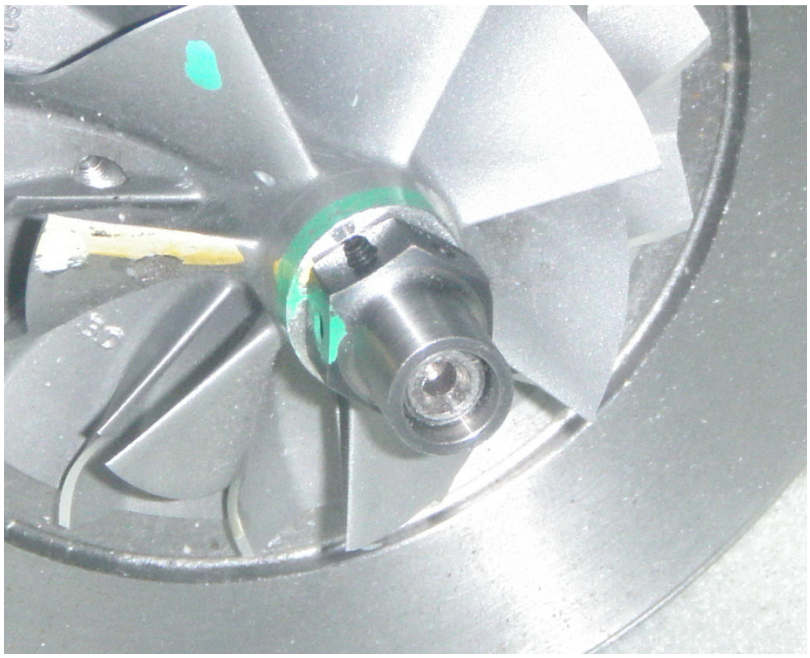

Figure 2.13. Close up of target nut.

Figures 2.14 and 2.15 show some additional pictures of the actual part and Figure 2.16 shows the wheel with the compressor cover on and a weight being installed. Figures 2.17 and 2.18 show the turbine.

Figure 2.14. Compressor wheel with allen key resting in an installed set screw.

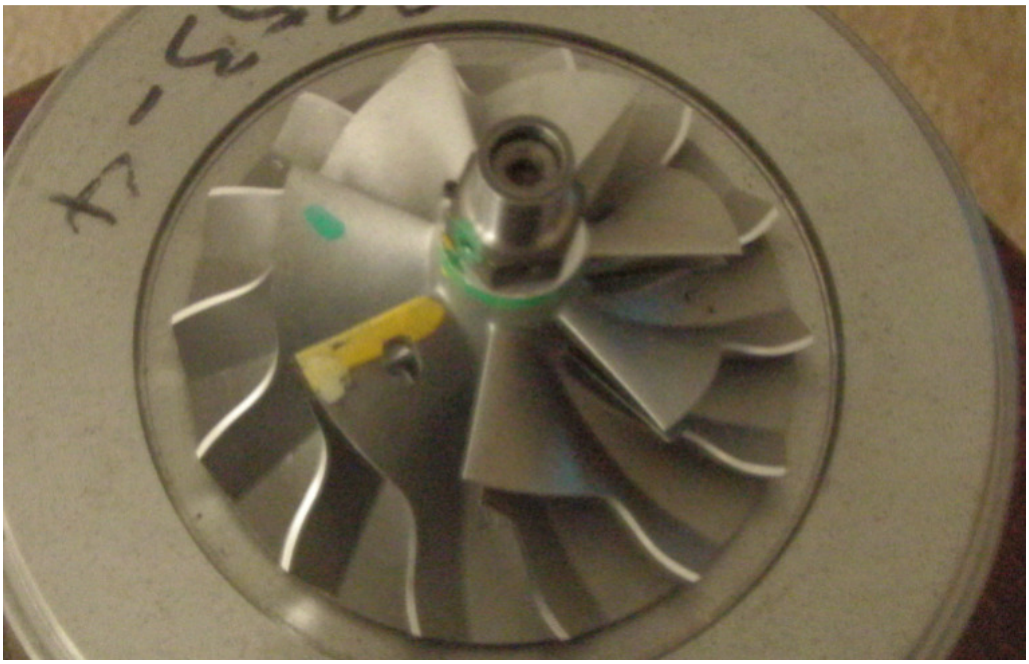

Figure 2.15. Overhead profile of compressor wheel.

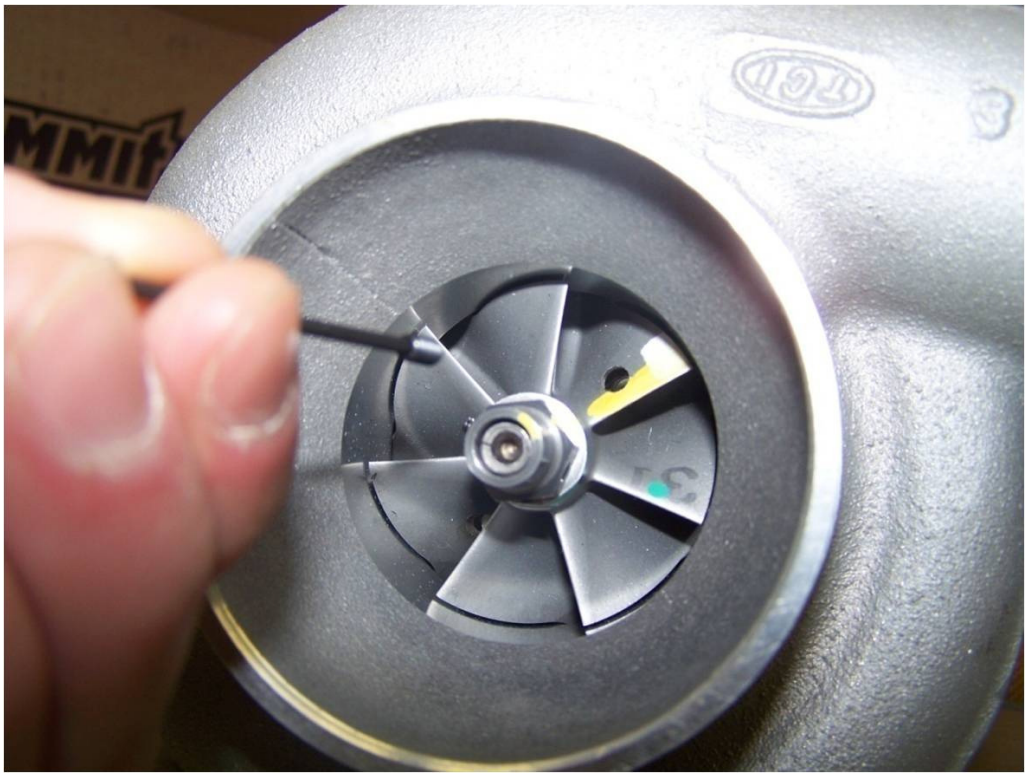

Figure 2.16. Installation of imbalancing weight.

Figure 2.17. Top profile for turbine.

Figure 2.18. Side profile of the turbine.

2.3 Experimental procedure

Due to the highly nonlinear nature of the system, no two runs will ever be exactly the same. Therefore, basic repeatability was at the forefront of the design of this experiment. Using custom ground set screws, a known distance, and a scale accurate to 0.005g, a range of unbalances were tested. The balance of the rotor with no weights in it is 0.15 g-mm, which is well below the functional or even nominal limits. A range of induced unbalance levels on both compressor and turbine were tested, from 0.342 g-mm up to 1.77 g-mm turbine and from 0.302 to 1.66 g-mm compressor. At these high levels of unbalance, the load on the bearings is in excess of 14 kg, while the entire rotor weighs only about 1 kg. Table 2.2 tabulates the unbalance combinations tested as well as the condensed pertinent data, in raw form, for reference.

Table 2.2. Test Matrix

Run #	Uc (g*mm)	Ut (g*mm)	Max Speed (RPM)	Max Subsync (mils)	Max Sync (mils)	Max Decel (mils)	Max Accel (mils)
12	0	0	82800	3.08	1.59	5.53	5.94
18	0.755	0	88180	3.06	2.85	3.9	5.37
19	0.755	0	91520	3.01	2.88	5.06	4.64
13	0.906	0	90000	3.44	2.8	4.37	5.78
14	0.906	0	86860	3.5	2.85	4.81	5.47
15	0.906	0	85840	3.37	2.88	5.29	6.06
21	0	1.77	90000	2.65	2	3.91	5.06
28	0	1.77	88860	2.62	2.08	5.53	5.22
29	0	1.77	87900	2.54	2.13	5.76	5.5
23	0.906	1.77	87840	2.4	2.98	5.29	5.83
24	0.906	1.77	90860	2.18	3	5.76	5.14
26	1.66	1.77	87840	1.85	3.96	5.29	5.78
30	0.906	1.062	86820	1.7	0.36	4.37	5.81
31	0.906	1.062	85120	1.54	0.334	3.55	5.29
32	0.906	1.062	81840	1.59	0.334	5.63	5.71
33	0.906	1.062	89600	2.7	0.36	NA	5.89
34	0.906	1.062	89600	2.02	0.334	NA	5.89
35	0	0.342	86840	2.21	1.95	5.99	5.22
36	0	0.342	89160	2.36	1.7	4.14	5.58
37	0	0.342	87540	2.31	1.75	5.06	5.47
38	0.302	0.342	85840	2.08	2.03	4.34	5.83
39	0.302	0.342	42600	1.93	2.08	5.94	5.35
43	0.604	0.342	88180	2.11	2.83	5.35	5.37
40	0.906	0.342	84800	2.03	2.78	3.83	5.45

Due to the temperature of the exhaust, it was much more straightforward to set unbalance levels in the turbine and change the compressor unbalance from run to run. Multiple runs were taken to ensure repeatability.

The engine was operated while connected to the eddy current dynamometer using a double flex joint drive coupling. The spectral waterfall plots of an engine acceleration and deceleration are shown in Figures 2.9 and 2.10, where the top speed of the turbo is noted to be

87510 rpm. These waterfalls are time steps of the frequency content read by the instrumentation. Timestamps are shown on the left y-axis, and the corresponding shaft speed on the right y-axis. The x-axis shows the frequency, and the height of the line is the amplitude of vibration. The engine vibrations remain in the lowest part of the frequency spectrum. It is not spinning nearly as fast as the turbocharger, so this is expected. Unstable modes, most likely a conical mode mixing with a rotating bending mode, are also evident in the figure. The synchronous vibration had well defined peaks with no sidebands and shows the integrity of the keyphasor signal.

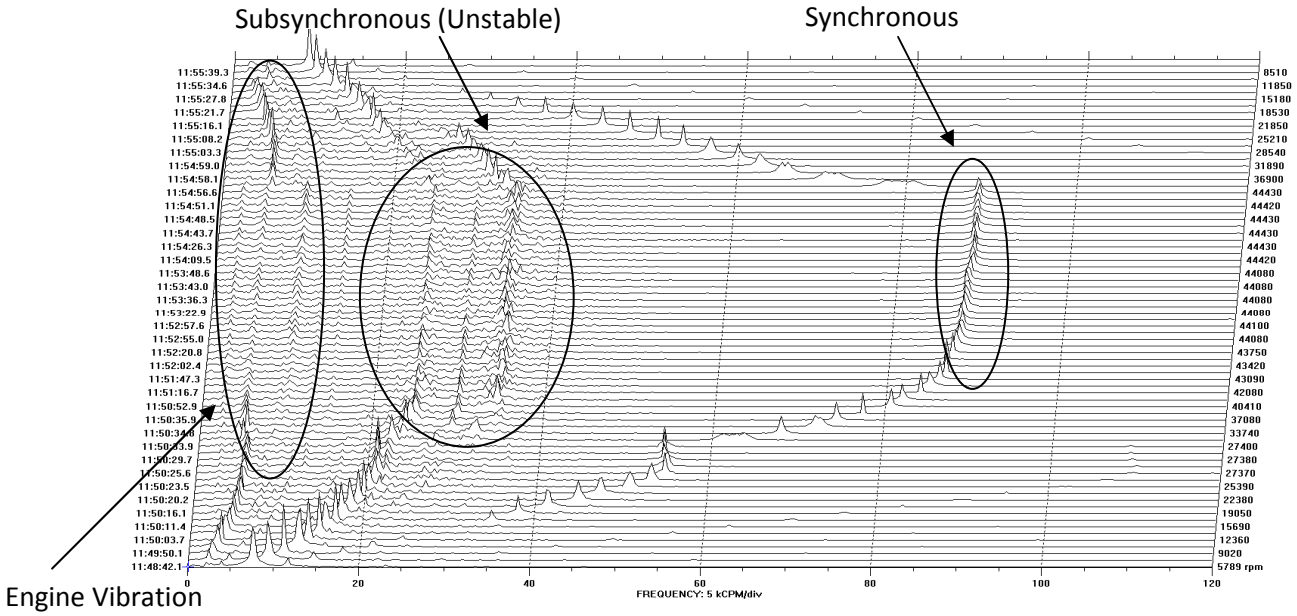

Figure 2.9. Spectrum content for no added unbalance (factory balance)
X-axis frequency scale shows correct turbo speed, 88860 rpm is the top turbo speed.
Reference speed shown on right scale is ½ actual rpm.

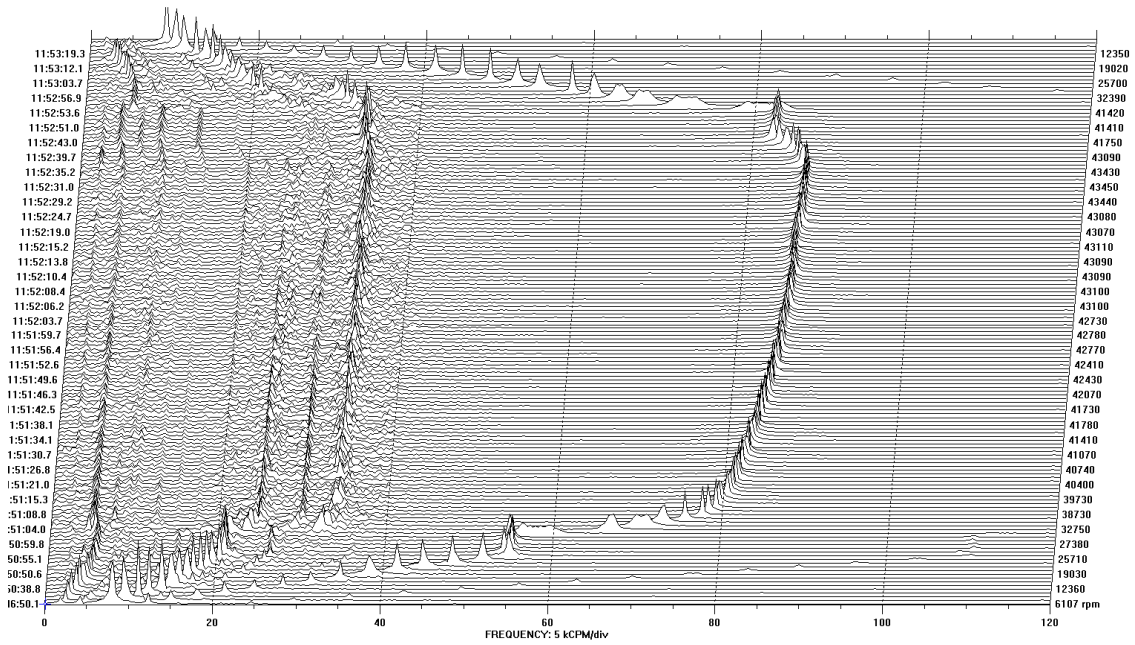

Figure 2.10. Spectrum content for compressor probe at full load test conditions
Uc= 0.906 g-mm, Ut=0 g-mm

For each testing period, the engine was allowed to idle and warm up to nominal operating temperature. Using a throttle handle attached to the DAQ cart, the engine was brought up to its maximum speed, 2800 RPM, then loaded to its maximum-power speed, 2500 RPM, and held until steady state. After steady-state was reached, the engine was allowed to run to test for any variations in steady state load. Transient acceleration and deceleration data were recorded as well.

Each run generated a spectral waterfall similar to ones seen in Figure 2.9 and Figure. 2.10 Each individual line was also accessible to allow accurate interpretation of the results, particularly finding the maximum amplitudes for each mode in each run. This means that the waterfall and spectrum plots contained the same data, just organized differently. To reiterate, the

waterfall plots are simply constructed by laying spectral plots down one after another in a time series. An example is shown in Fig. 2.19.

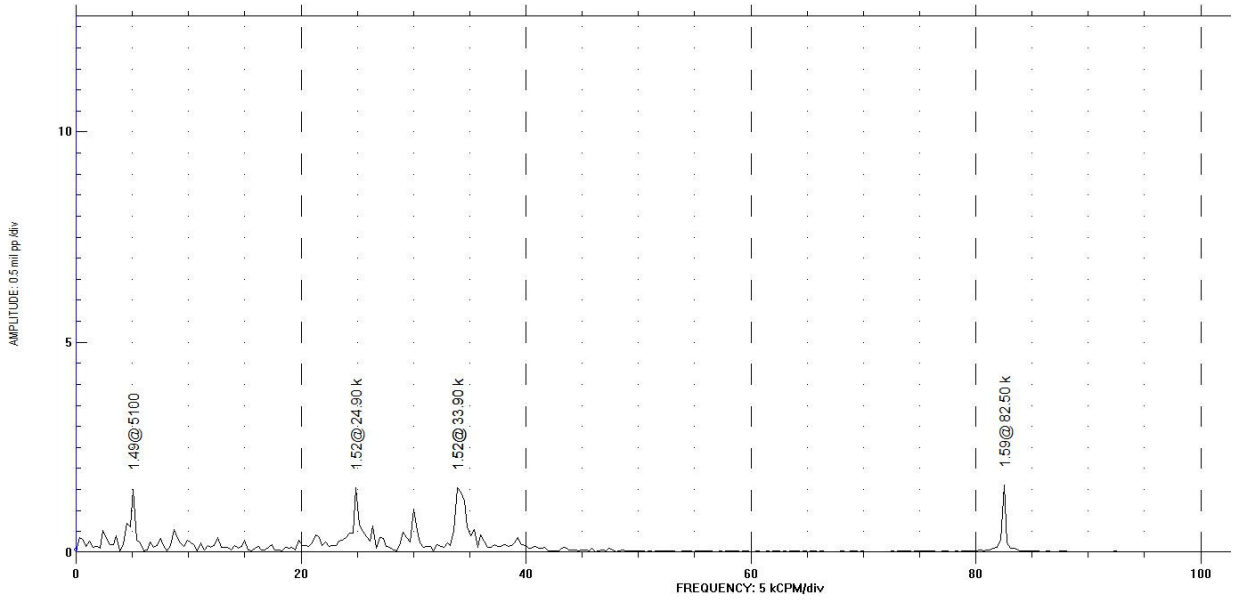

Figure 2.19. Spectral plot for no added unbalance**.**

Chapter 3

Results and Discussion

This section presents the outcome of the experiment. The results are organized by turbine balance level because that is the end that was shown to have the most effect on the system. For each turbine balance level, the range of compressor imbalance levels is reported on the horizontal axis. The corresponding maximum amplitudes for both synchronous and subsynchronous vibration are given. A set of the charts organized by compressor balance not practical because the balances set on the compressor were not as regular as the turbine balance settings were.

The results are encouraging, but more unbalance resolution, in-depth phase analysis, and additional measurement positions are all going to be necessary before any firm conclusions can be reached. However, there are still several patterns that merit discussion. The results for loaded steady state and transient acceleration and deceleration are tabulated and presented, organized by turbine balance.

3.1 Steady State Response

The no added unbalance case is contained in Figure 3.1. It shows a range of compressor unbalances with no weights in the turbine. Of note is the level of vibration for the null case, with an extremely low harmonic component, and a maximum subsync level of about 3 mils. Once unbalance is added, the sync increases to a higher level as expected. The subsync appears to remain mostly unaffected by the addition of unbalance for this case.

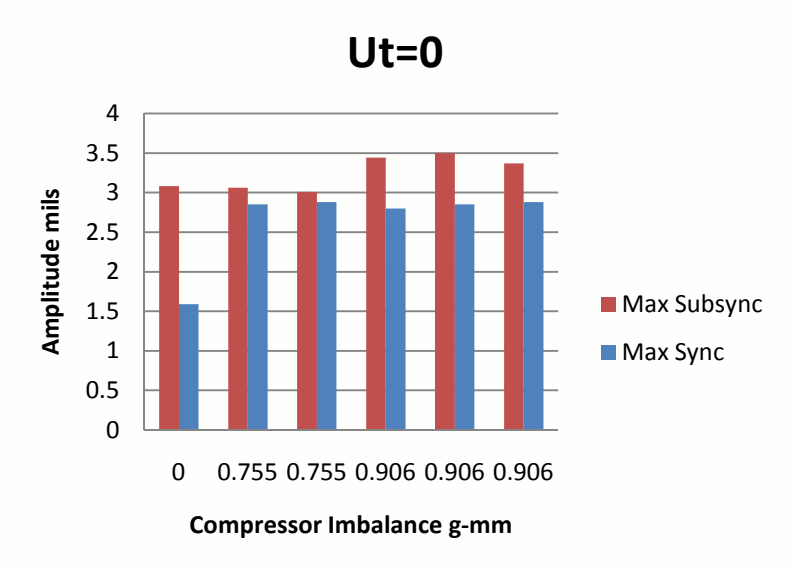

Figure 3.1. Target nut amplitude. Steady-state, full load.
Ut= 0, x-axis is compressor unbalance level

The addition of imbalancing weight to the turbine in Figure 3.2 showed promising results. The compressor target nut measurement showed reduced levels of both synchronous and subsynchronous vibration levels. Note that the increase in imbalance reduced subsync levels by almost a third.

Once again, the changing compressor unbalance did not appear to have much effect on the overall vibration levels. Increased levels of unbalance on the compressor end in Figure 3.2 did increase the synchronous amplitudes, but when compared to Figure 3.1, the levels remain mostly the same. It is, in fact, that the rest of the amplitudes have been reduced.

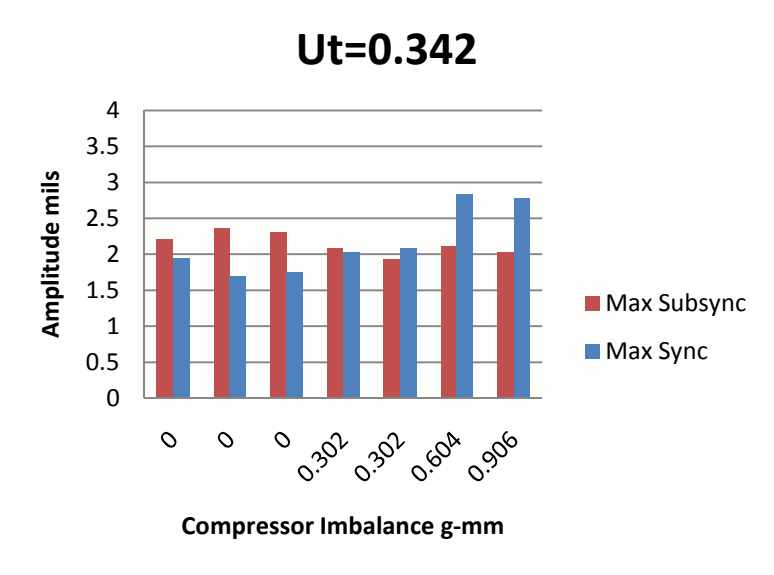

Figure 3.2. Target nut amplitude. Steady-state, full load.
Ut= 0.342, x-axis is compressor unbalance level

Figure 3.3 shows the response to high levels of imbalance on the turbine. Addition of heavy levels of unbalance had the expected effect, increasing the levels of harmonic vibration as it increased. Subsynchronous vibration decreases with the addition of turbine unbalance as expected, and continues to decrease even more with the addition of weights to the compressor. As usual, the sync increases with addition of unbalance. It is interesting to note how the subsync decreases with the addition of this mass.

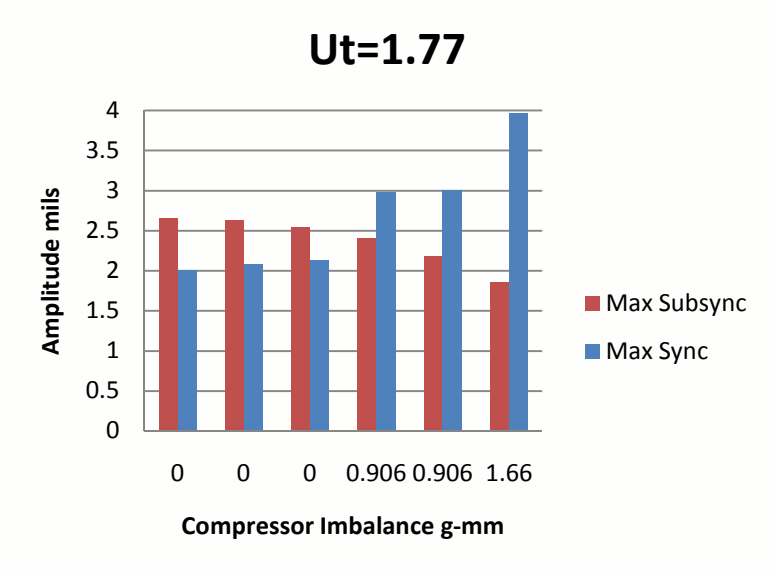

Figure 3.3. Target nut amplitude. Steady-state, full load.
Ut= 1.77 g-mm, x-axis is compressor unbalance level

In It is worth noting that the Ut=0(Fig 3.1) case contained the most violent subsynchronous vibrations. This is interesting because it implies that it is possible for a rotor to have *insufficient* unbalance to be useful in an industrial application due to the presence of what could be extremely damaging subsync levels. When Ut=0.342 (Fig 3.2), it is encouraging to see that the subsync levels decrease by about 30%. This lends credence to the idea that induced unbalance can reduce the maximum subsync levels. At high unbalance of Ut=1.77(Fig 3.3), the overall subsync level increases again, though not to the Ut=0 levels. This is likely due to other effects that were exacerbated with such high amounts of mass eccentricity. A second look at the trending in Figure 3.3 shows clearly that even though the overall subsync increased, the addition of unbalance decreased the subsync from run to run.

3.2 Transient Response

Although an engine may be rated in terms of its maximum power and a loaded condition, it will still go through many accelerations and decelerations. In addition to the fact that the highest amplitudes seen were during transient conditions, this makes the transient condition a worthwhile area of study.

The harmonic amplitudes were low in transient testing, and therefore not included in the following graphs. The subsynchronous amplitudes though, particularly in the first whirl mode, were significantly higher. They were higher than any amplitude found during full load as well. Figures 3.6, 3.7, and 3.8 below illustrate the transient response, organized in the same manner as the steady state response.

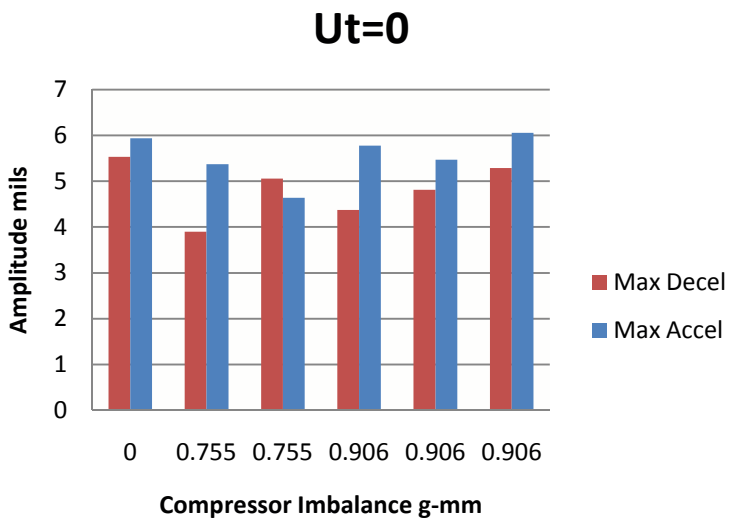

Figure 3.6. Target nut amplitude. Transient response. Ut=0, x-axis is compressor unbalance

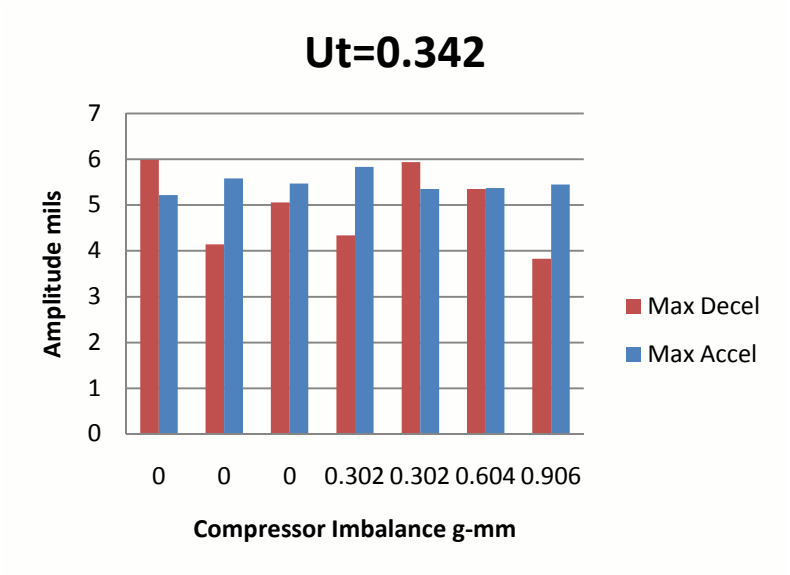

Figure 3.7. Target nut amplitude. Transient response.
Ut=0.342, x-axis is compressor unbalance

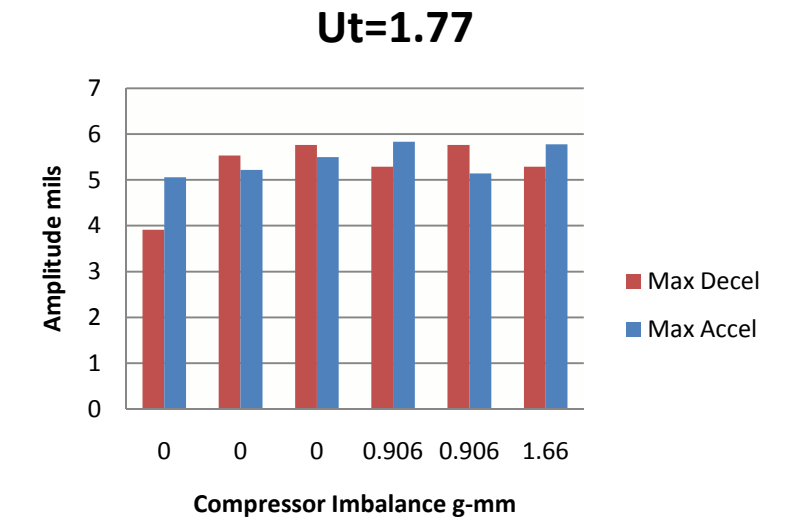

Figure 3.8. Target nut amplitude. Transient response.
Ut=1.77, x-axis is compressor unbalance

The trends are not as clear in the transient cases. The only thing that is clear is that the overall amplitudes are significantly greater than the steady state. The overall averages remain

close to 5 mils, much higher than anything seen in the fully loaded case. This is understandable in the fact that acceleration itself is manifested as a destabilizing force, especially when considering the changing aerodynamic loading. Much more study is needed in this area as the effect of many different parameters is still in question. Some examples are compressor-turbine mass ratio, acceleration rate, and oil flow rate.

3.3 Limitations and future work

There are many avenues available to continue work in this field. At this point in the research, finer unbalance levels could still be tested in more rigorous combinations to look for trends in tighter bands of unbalance.

The engine's ability to spin this particular turbocharger has been an issue throughout the experiment. A second subsynchronous mode comes in around 75krpm, and the engine is only capable of spinning the turbine to about 91krpm, and not at all balance levels. This mode appears to have higher overall amplitudes and is likely to be the problem-causing mode during loaded operation. A more powerful engine or smaller wheel setup could possible alleviate the problem. Another option is that due to the relative invariability of the compressor unbalance, a new, smaller compressor could be tested against the same turbine unbalances to investigate the second subsynchronous mode.

Additional methods of testing could be implemented in order to study the transient effects more closely. For example, the engine could be loaded at 1200 RPM, and let the dyno accelerate it to 2500 RPM, instead of, or in addition to, the current method.

Future experiments on this test stand could also include an analysis of the specific sensitivity of each mode. Certain modes may be more or less affected by turbine vs compressor

unbalance, or possibly have minimums in a small range of unbalance. These modes may also be affected by the relative weight along the rotor, one specific example being the use of titanium or aluminum for the compressor.

Determining the sources of the frequency components is always an area of interest in spectral analysis. The dynamic instability is caused by bearings but there are other candidates for the sources of the lesser vibrations, such as aerodynamic volute loading or oil pressure.

Another consideration is the placement of weights with respect to phase. More study would investigate the response of having unbalance in phase or out of phase. It is theorized that in phase would increase the first cylindrical mode, while being 180° out of phase would increase conical modes. This would be useful knowledge as the reduction of unstable vibration by a means as simple as properly clocking the wheels would be extremely valuable.

Finally, and maybe most importantly, a method for mid-shaft measurement should be investigated. Figures 3.4 and 3.5 demonstrate an additional case worth considering. It was repeated five times to ensure its reliability. It was the lowest overall vibration encountered in the entire experiment. Even with a fair amount of unbalance on both ends of the rotor, the synchronous vibration was extremely low. This illustrates the limitations of using the compressor nut as the only source of measurement. These readings are not likely to be representative of the vibration of the whole rotor. It is worth noting that, in Figure 3.5, the amplitude of subsync is higher in the last two readings because of a slightly higher achieved turbo speed, moving into the second, more unstable, mode.

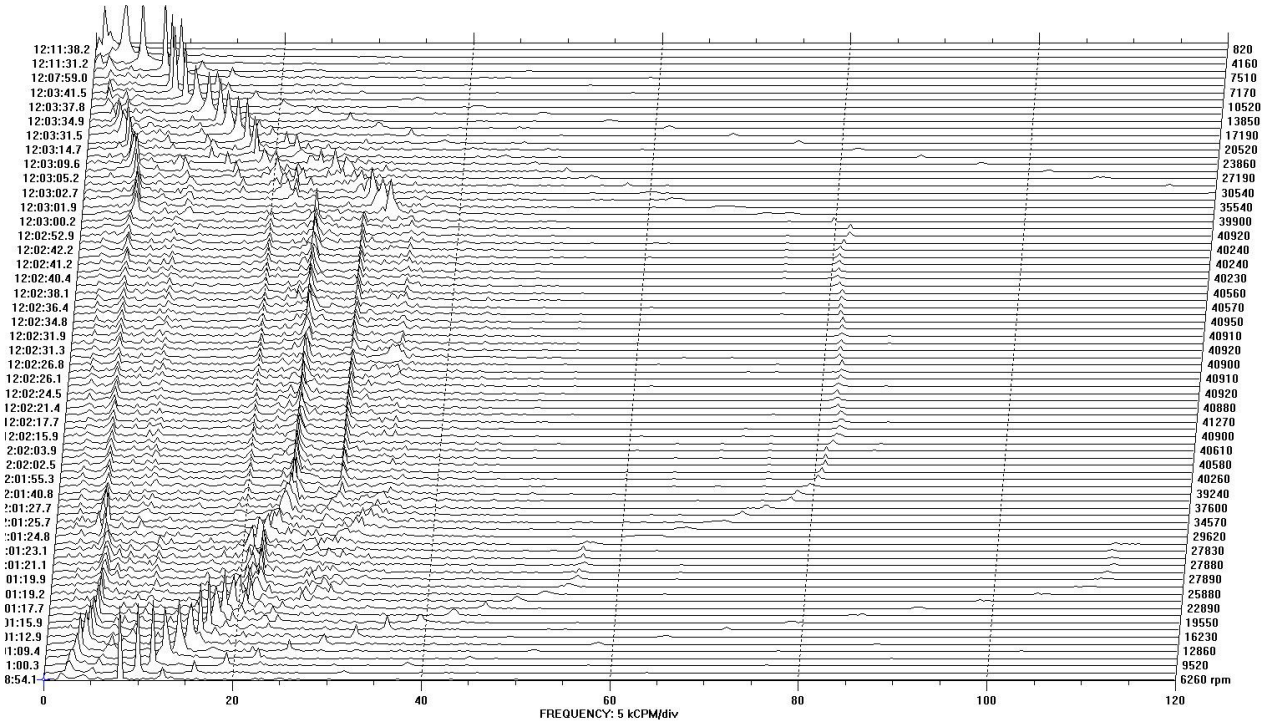

Figure 3.4. Waterfall for Ut=1.062, Uc=0.906. Note the extremely low levels of sync.

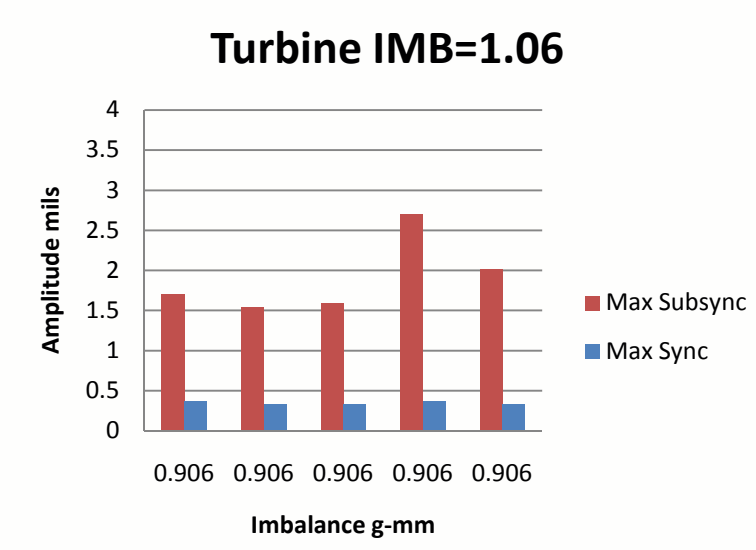

Figure 3.5. Vibration levels for Ut=1.062, Uc=0.906

Having only one place to measure is very limiting, and the compressor nut is not an ideal place to take a reading. Several reasons compound this problem. The relative lightness of the compressor

end makes it difficult to use to predict the motion of the entire shaft. However, the rest of the shaft is difficult to instrument; it is either bathed in oil or extremely hot. Designs for mid-shaft measurement have been conceptualized, but not implemented on the OEM turbocharger. However, that turbo has not been modified to allow the addition of variable unbalance conditions.

3.4 Conclusions

Almost all turbochargers exhibit unstable behavior throughout their operating range. This phenomenon is constantly being combated in industry, as these instabilities can lead to losses in time and money. This research planned to show what the effect of induced unbalance was on subsynchronous vibration.

The experimental evidence shown here agrees with the past analytical and numeric predictions that the addition of unbalance can suppress the appearance of subsynchronous vibration. From a practical standpoint, it is good to realize that there is a lower limit to the benefits of balancing a rotor. This is useful because balancing a rotor, often in several planes, to a limit of zero is not practical. More study is needed to decide exactly how much unbalance to leave on the rotor, but that is likely to vary with geometry and specific conditions. Hopefully, these results will lead to more directly controllable aspects of rotordynamic design that can be used to suppress subsynchronous vibrations in the future.

REFERENCES

[1] Watson, N. and Janota, M. S., 1982, *Turbocharging the Internal Combustion Engine*, Wiley, New York.

[2] Gunter, E. G. and Chen, W. J., 2005, "Dynamic Analysis of a Turbocharger in Floating Bushing Bearings," *Proc. 3rd International Symposium on Stability Control of Rotating Machinery*, Cleveland, OH.

[3] Gunter, E. G. and Chen, W. J., 2000, *DyRoBeS© - Dynamics of Rotor Bearing Systems User's Manual*, RODYN Vibration Analysis, Inc., Charlottesville, VA.

[4] Ehrich, F. F., 1999, *Handbook of Rotordynamics*, Krieger Pub. Co., Malabar, FL.

[5] Holmes, R., Brennan, M. J. and Gottrand, B., 2004, "Vibration of an Automotive Turbocharger – A Case Study," *Proc. 8th International Conference on Vibrations in Rotating Machinery,* Swansea, UK, pp. 445-450.

[6] Li, C. H. and Rohde, S. M., 1981, "On the Steady State and Dynamic Performance Characteristics of Floating Ring Bearings," *Trans. ASME Journal of Lubrication Technology*, **103**, pp. 389-397.

[7] Shaw, M. C. and Nussdorfer, T. J., 1947, "An Analysis of the Full-Floating Journal Bearing," Report No. 866, National Advisory Committee for Aeronautics (NACA).

[8] Kirk, R. G., 1980, "Stability and Damped Critical Speeds: How to Calculate and Interpret the Results," *Compressed Air and Gas Institute Technical Digest*, **12**(2), pp. 1-14.

[9] Tanaka, M., Hatakenaka, K. and Suzuki, K., 2002, "A Theoretical Analysis of Floating Bush Journal Bearing with Axial Oil Film Rupture Being Considered," *Trans. ASME Journal of Tribology*, **124**, pp. 494-505.

[10] Alsaeed, A. A., 2005, "Dynamic Stability Evaluation of an Automotive Turbocharger Rotor-Bearing System," M.S. Thesis, Virginia Tech Libraries, Blacksburg, VA.

[11]Swanson, E., 2005, "Fixed-Geometry, Hydrodynamic Bearing with Enhanced Stability Characteristics," *STLE Tribology Transactions*, **48**(1), pp. 82-92.

[12] Born, H. R., 1987, "Analytical & Experimental Investigation of the Stability of the Rotor-Bearing System of New Small Turbocharger," *Proc. Gas Turbine Conference and Exhibition*, Anaheim, CA, 10p.

[13] Andres, L. and Kerth, J., 2004, "Thermal Effects on the Performance of Floating Ring Bearings for Turbochargers," *Proc. Instn Mech Engrs J Engineering Tribology*, 218(J), pp 437-450.

[14] Kirk, R.G., Alsaeed, A.A. and Gunter, E.J., 2007, "Stability Analysis of a High-Speed Automotive Turbocharger," *Tribology Transactions*, **50**(3), pp 427-434.

[15] Kirk, R. G., Alsaeed, A., Liptrap, J., Lindsey, C., Sutherland, D., Dillon, B., Saunders, E., Chappell, M., Nawshin, S., Christian, E., Ellis, A., Mondschein, B., Oliver, J., and Sterling, J., "Experimental Test Results for Vibration of a High Speed Diesel Engine Turbocharger," Tribology Transactions, 51(4), 2008, pp 422 - 427.

[16] Kirk, R. G., A. Kornhauser, J. Sterling, and A. Alsaeed , "Turbocharger On-Engine Experimental Vibration Testing," ASME Journal of Vibration and Control, in press, 2009.

[17] Kirk, R. G., J. Sterling, R. Utara, G. Biggins, D. Hodge, S. Johnson, J. Dean, B. Mastropieri, L. Fernandez, R. Rumeet, T. Miles, F. Chen, A. Johnson, H. Ko, A. Riggs, M. Price, and A. Cerni, "Diesel Engine Turbocharger Rebuild and Experimental Testing," ASME/STLE International Joint Tribology Conference, paper IJTC2007-44417, San Diego, CA, Oct 22-24, 2007

[18] Kirk, R. G., "Transient Journal Bearing Analysis," M.M.E. thesis, Department of Mechanical Engineering, University of Virginia, Charlottesville, Virginia, May, 1969.

[19] Kirk, R. G., and E. J. Gunter, Jr., "Transient Journal Bearing Analysis," NASA CR 1549, Federal Scientific and Technical Information, Springfield, Virginia 22151, June, 1970

APPENDIX A

Waterfall Plots for Each Significant Run

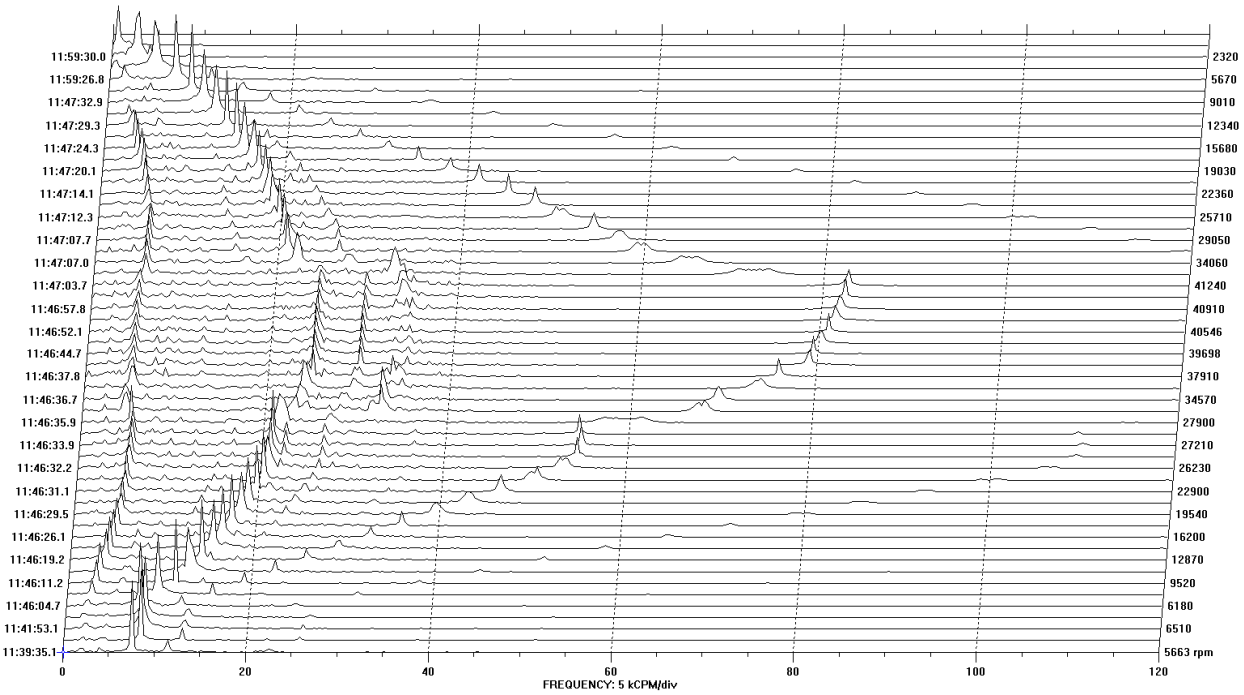

Figure A.1 Run 12, Ut=0, Uc=0, Nmax=82800 RPM

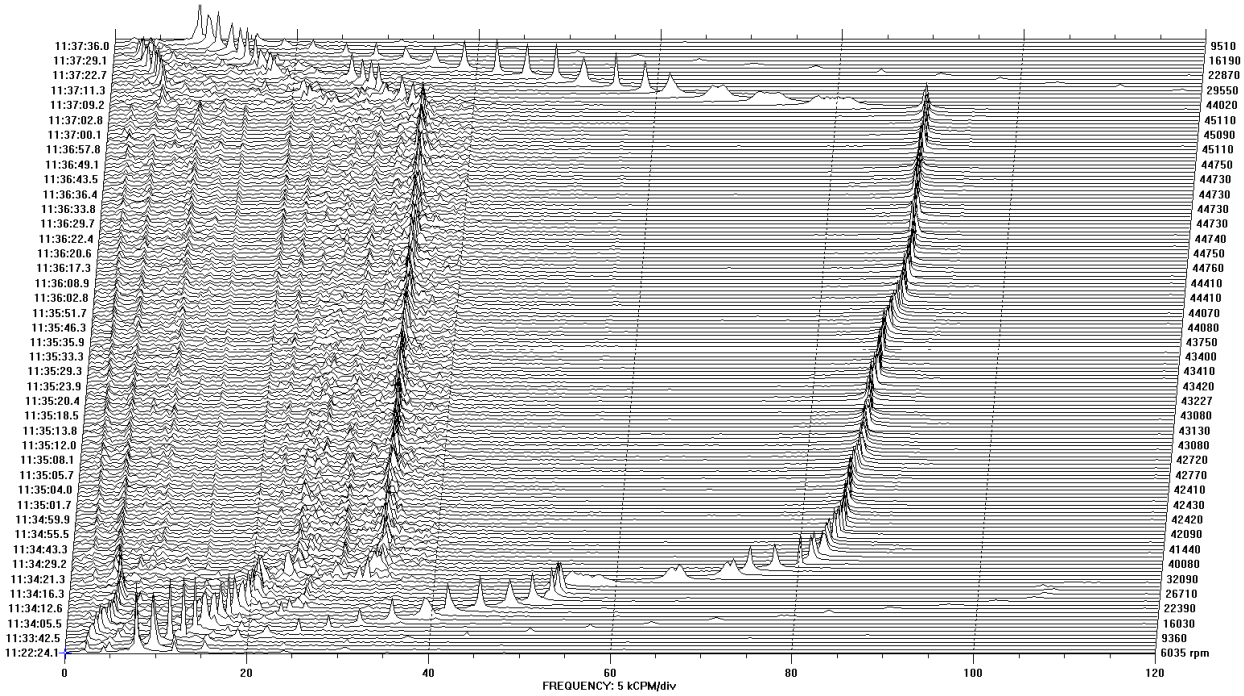

Figure A.2 Run 13, Uc=0.906 g-mm, Ut= 0, Nmax=90000 RPM

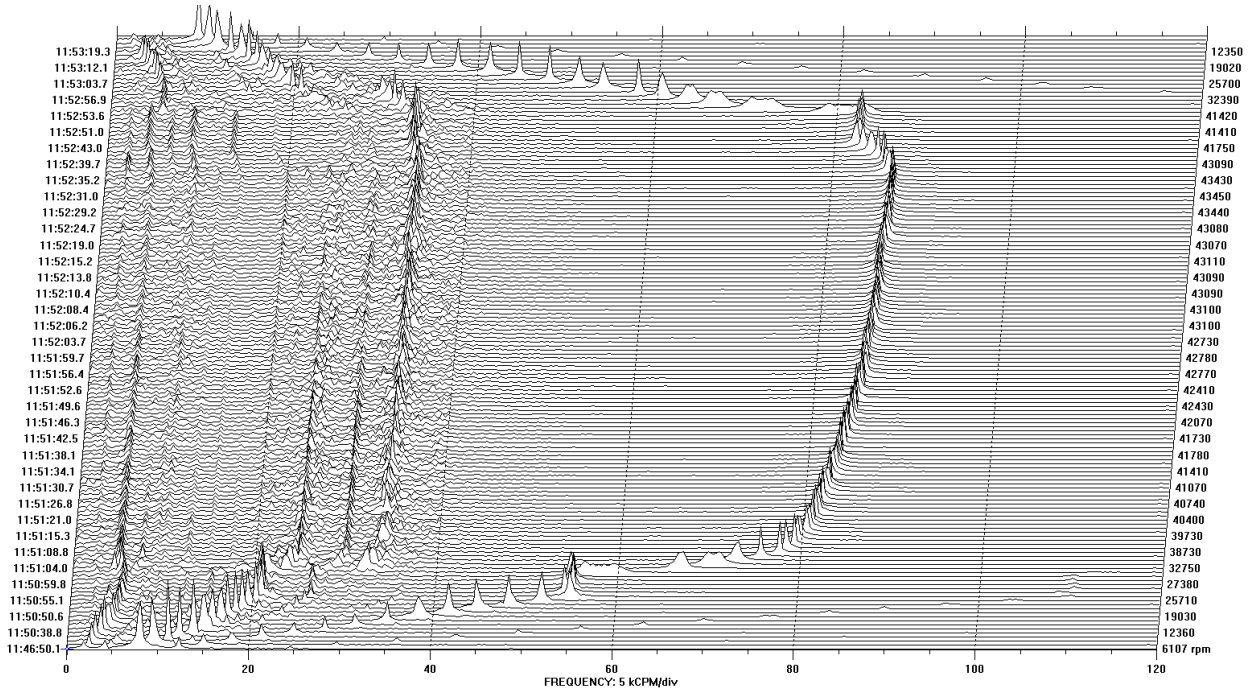

Figure A.3 Run 14, Uc=0.906 g-mm, Ut=0, Nmax=86860 RPM

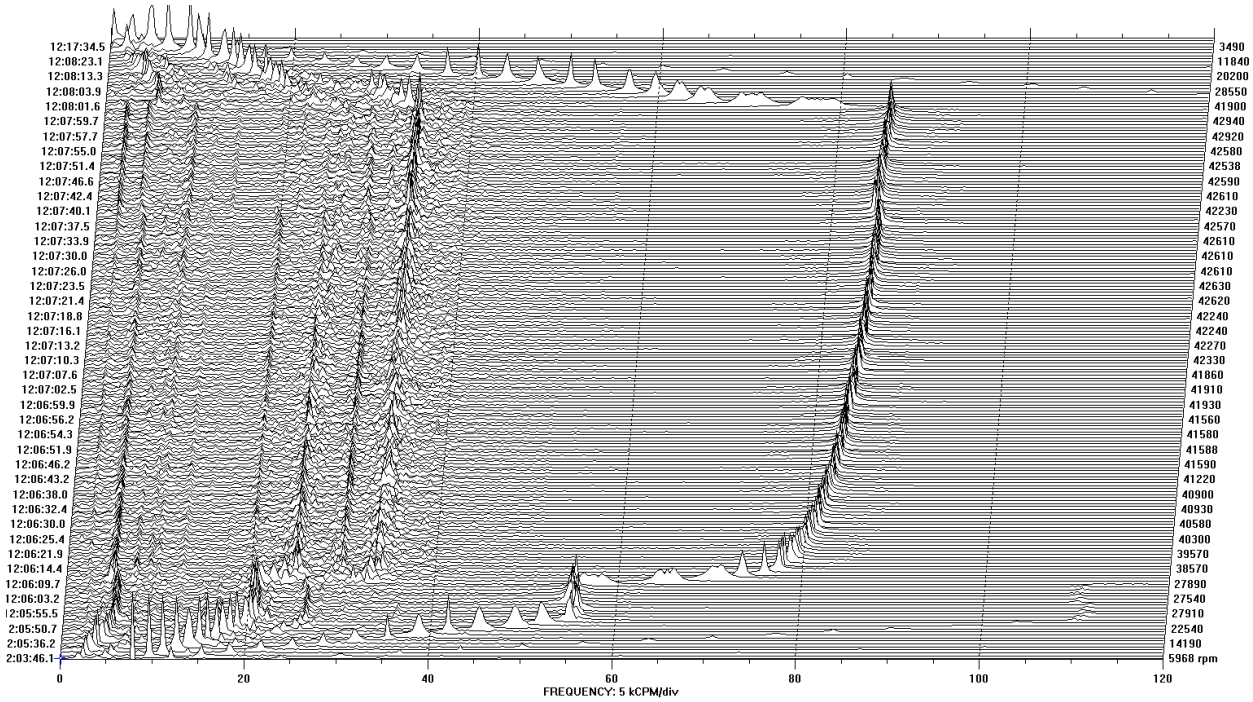

Figure A.4 Run 15, Uc=0.906 g-mm, Ut=0, Nmax=85840 RPM

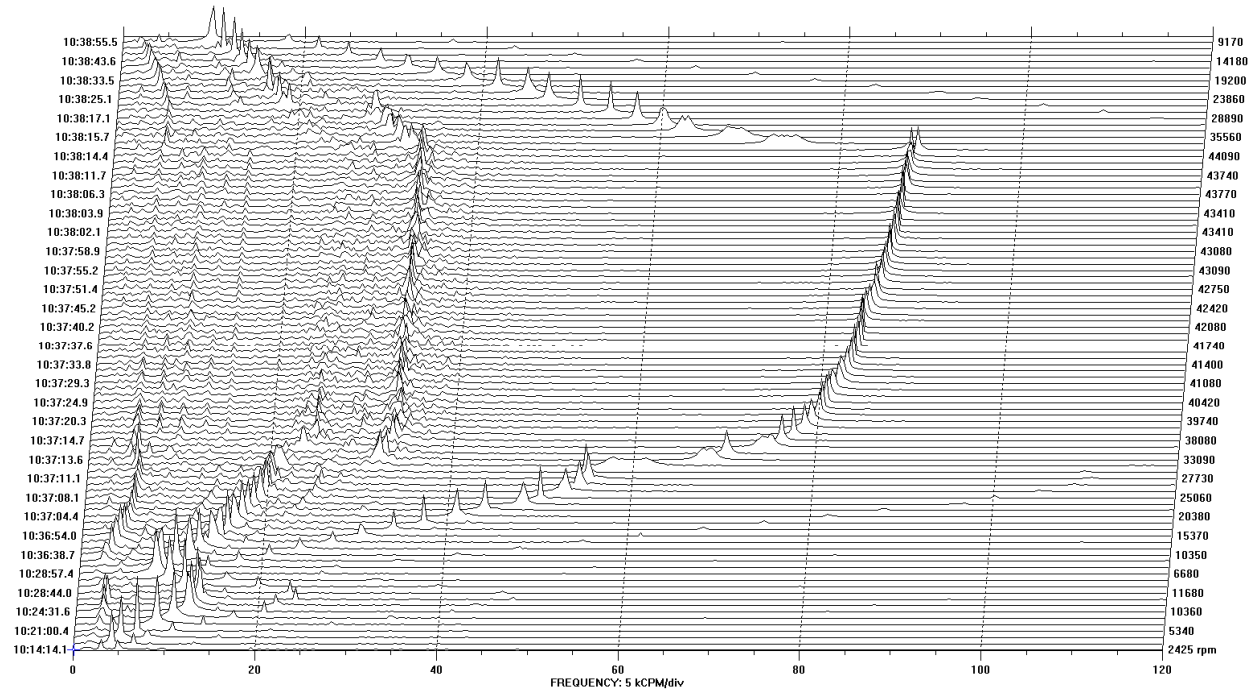

Figure A.5 Run 18, Uc=0.755 g-mm, Ut=0, Nmax= 88180 RPM

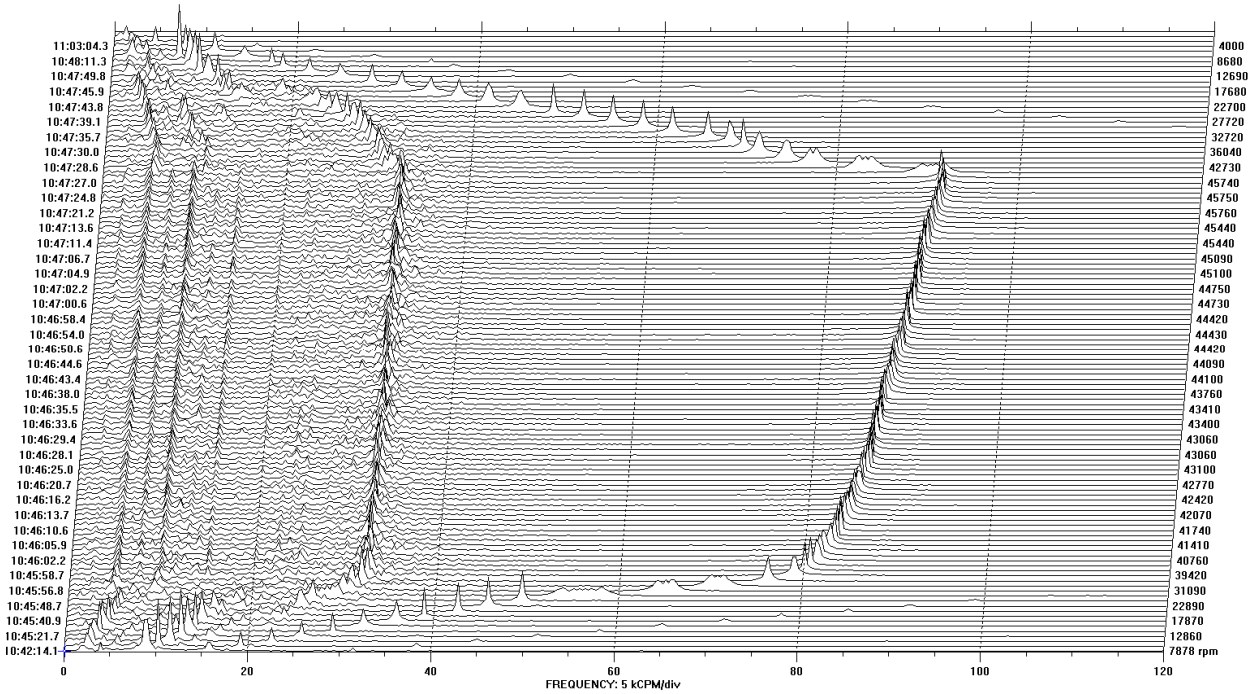

Figure A.6 Run 19, Uc=0.755 g-mm, Ut=0, Nmax=91520 RPM

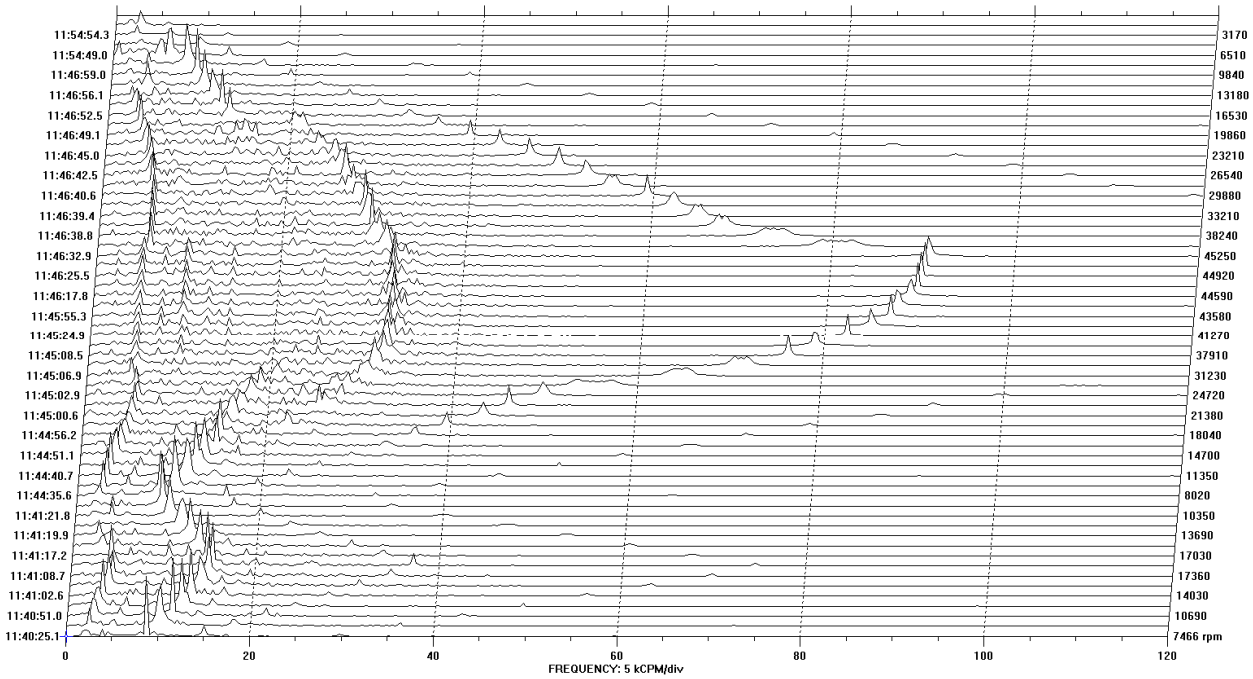

Figure A.7 Run 21, Uc=0, Ut=1.77 g-mm, Nmax=90000 RPM

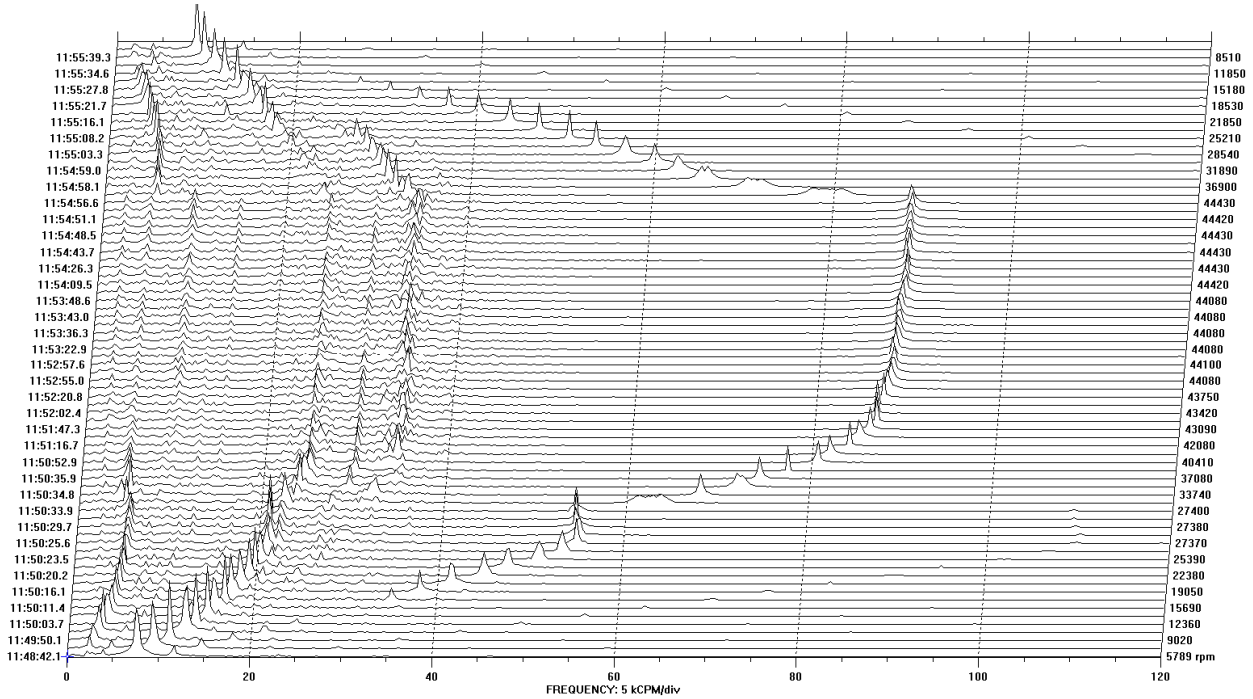

Figure A.8 Run 28, Uc=0, Ut=1.77 g-mm, Nmax=88860 RPM

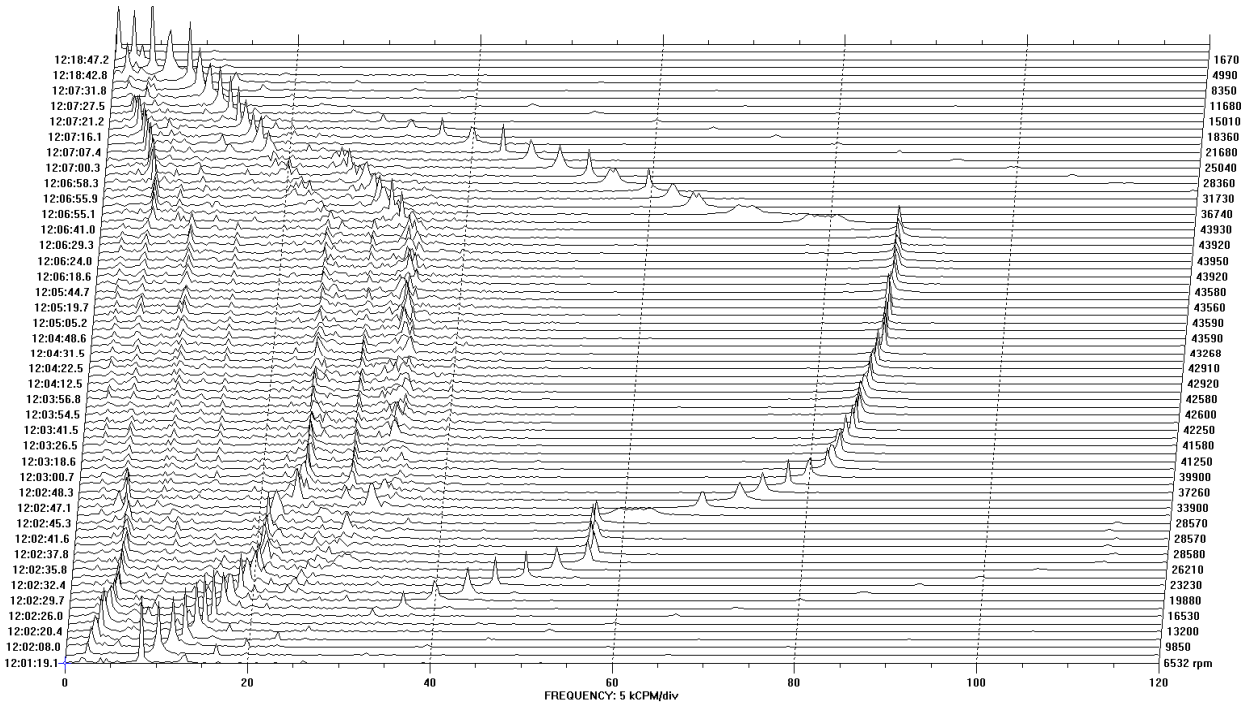

Figure A.9 Run 29, Uc=0, Ut=1.77 g-mm, Nmax=87900 RPM

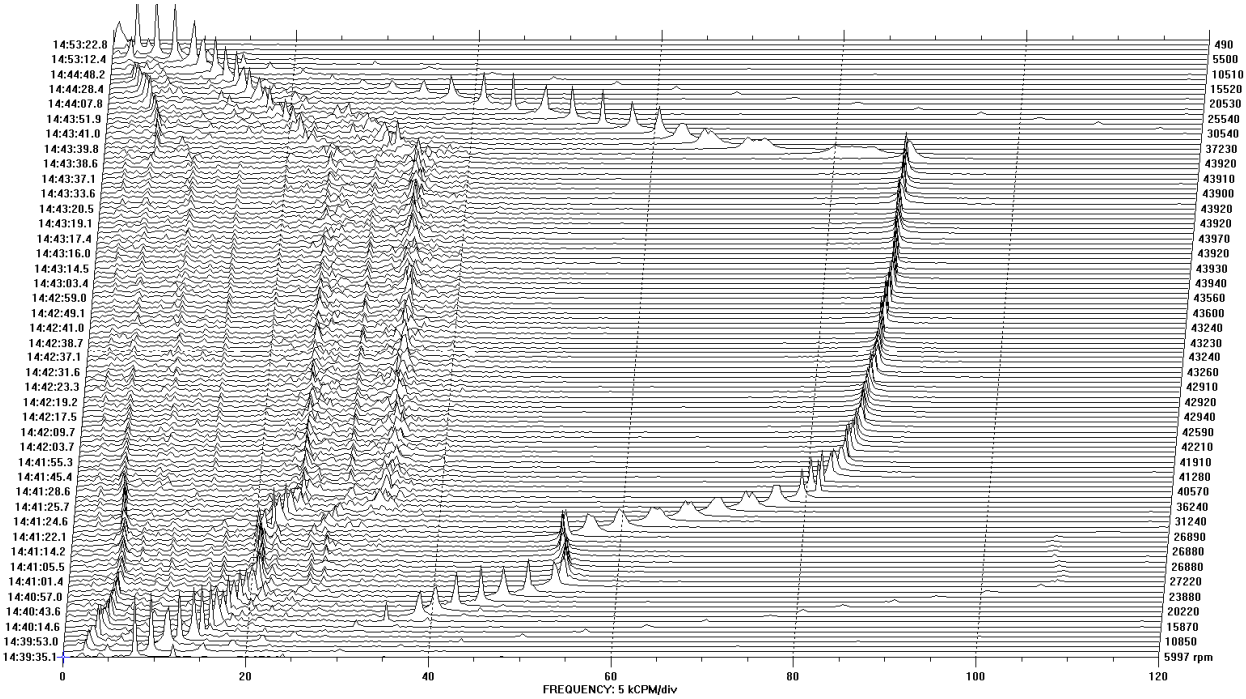

Figure A.10 Run 23, Uc=0.906 g-mm, Ut=1.77 g-mm, Nmax=87840 RPM

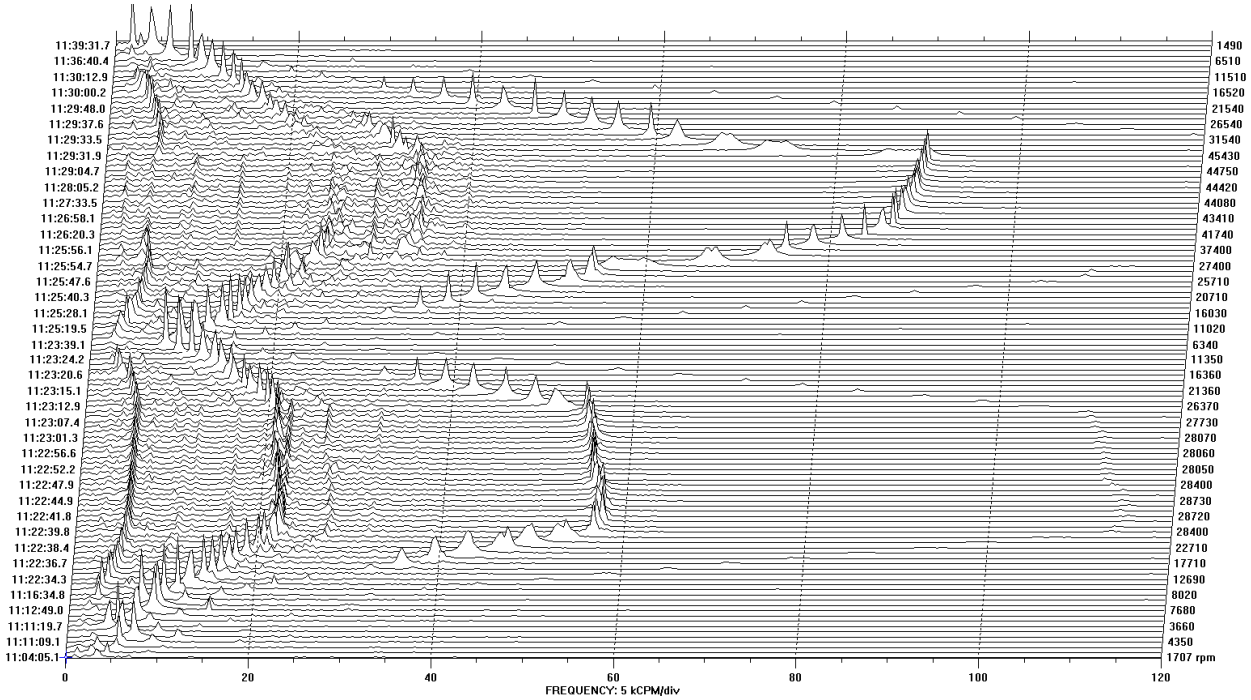

Figure A.11 Run 24, Uc=0.906 g-mm, Ut=1.77 g-mm, Nmax=90860 RPM

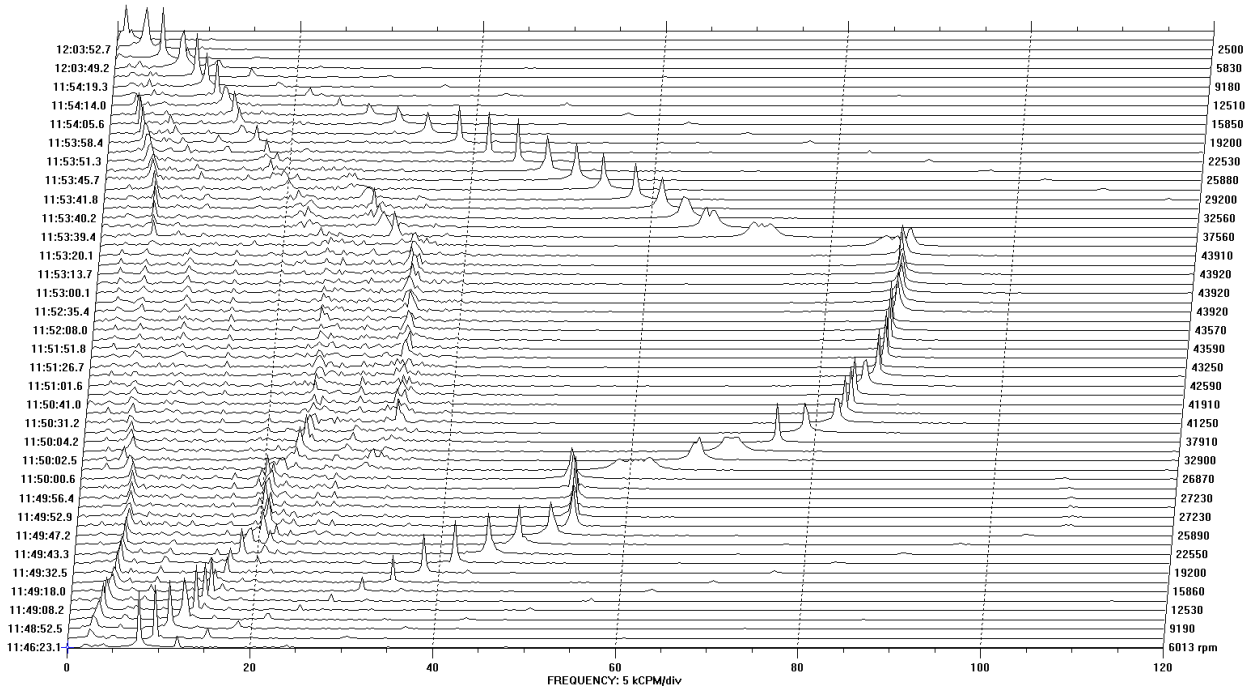

Figure A.12 Run 26, Uc=1.66 g-mm, Ut=1.77 g-mm, Nmax=87840 RPM

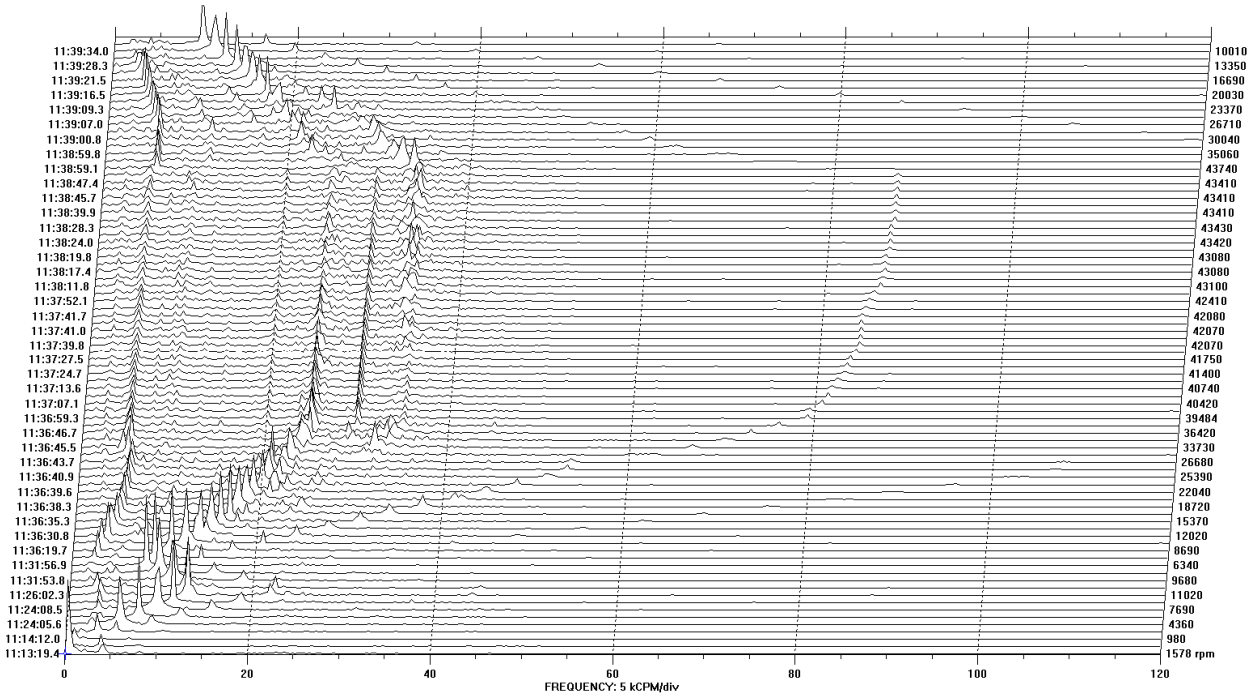

Figure A.13 Run 30, Uc=0.906 g-mm, Ut=1.062 g-mm, Nmax=86820 RPM

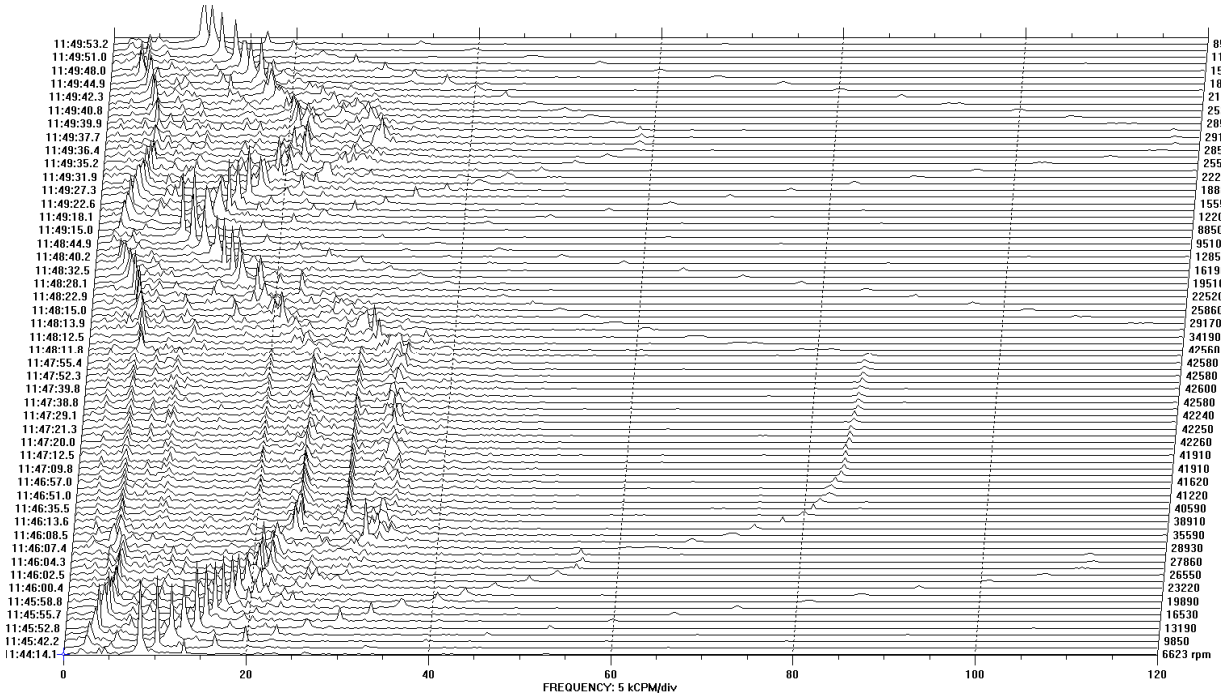

Figure A.14 Run 31, Uc=0.906 g-mm, Ut=1.062 g-mm, Nmax 85120 RPM

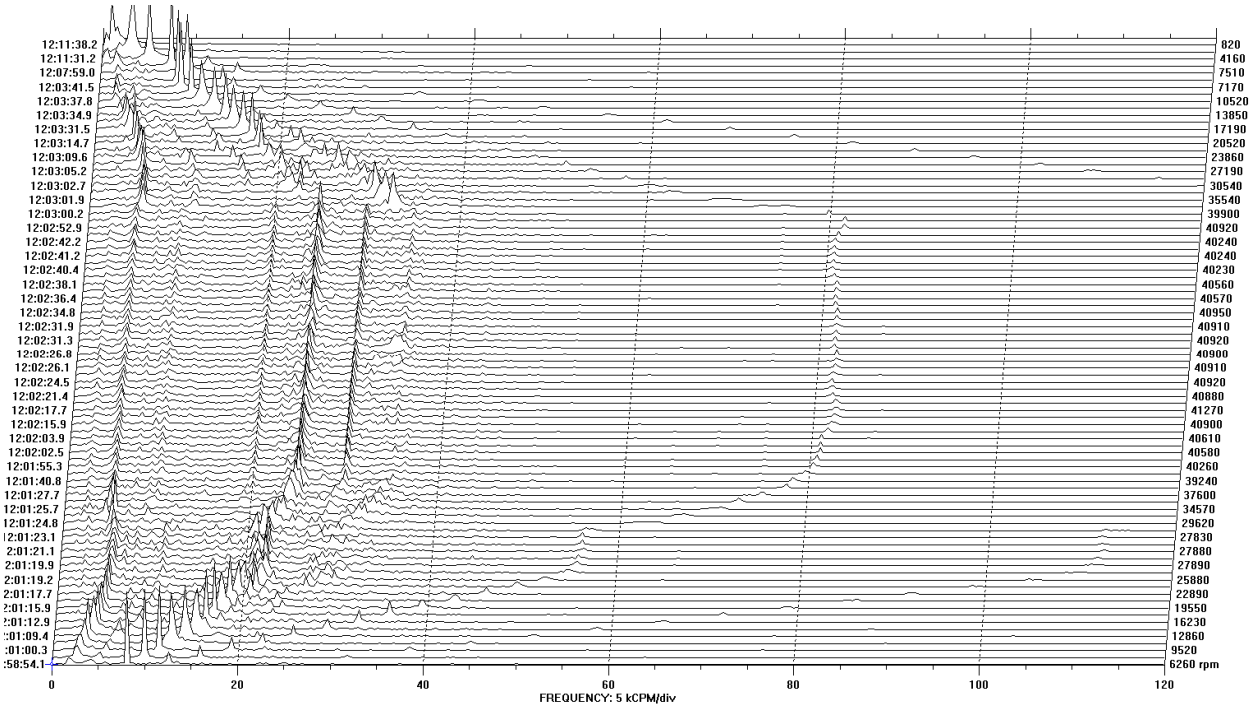

Figure A.15 Run 32, Uc=0.906 g-mm, Ut= 1.062 g-mm, Nmax= 81840

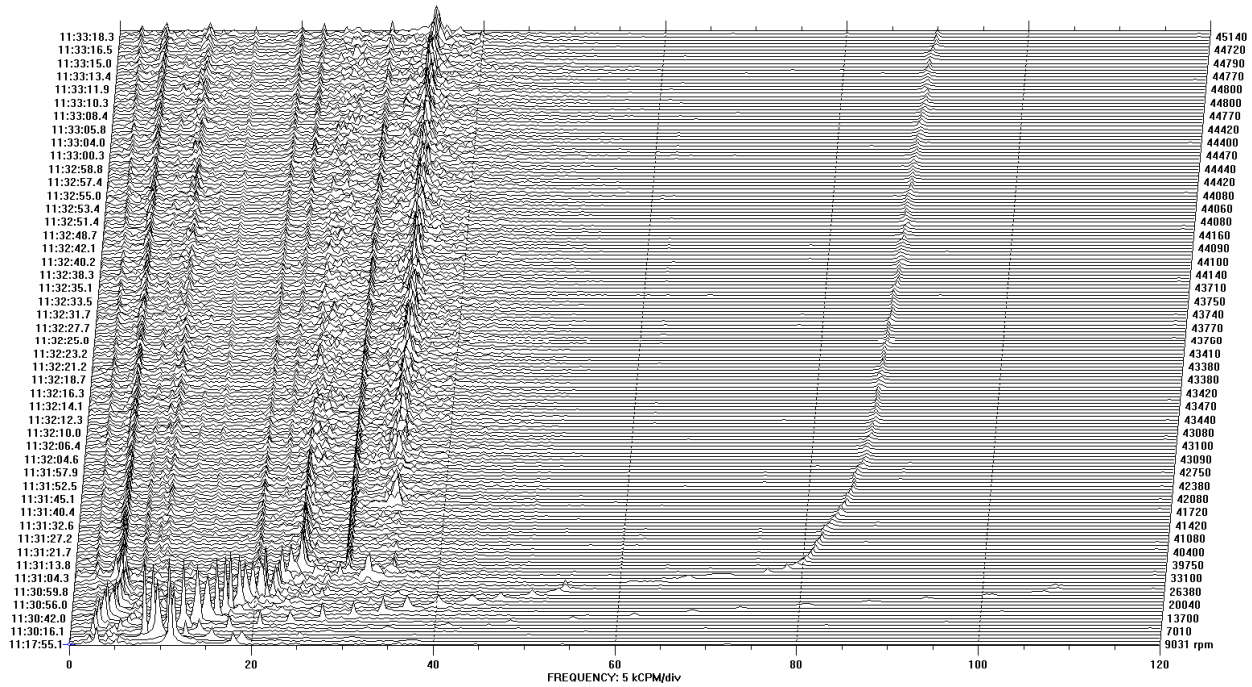

Figure A.16 Run 33, Uc=0.906 g-mm, Ut=1.062 g-mm, Nmax=89600 RPM

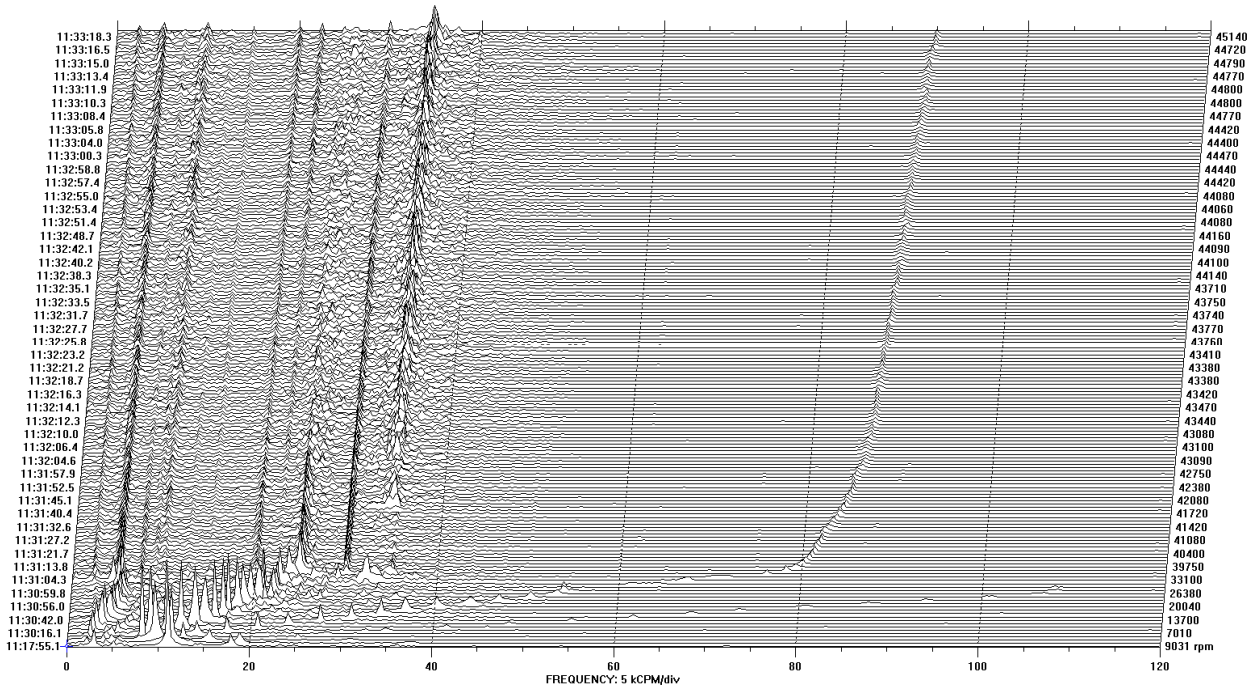

Figure A.17 Run 34, Uc=0.906, Ut=1.062 g-mm, Nmax=89600 RPM

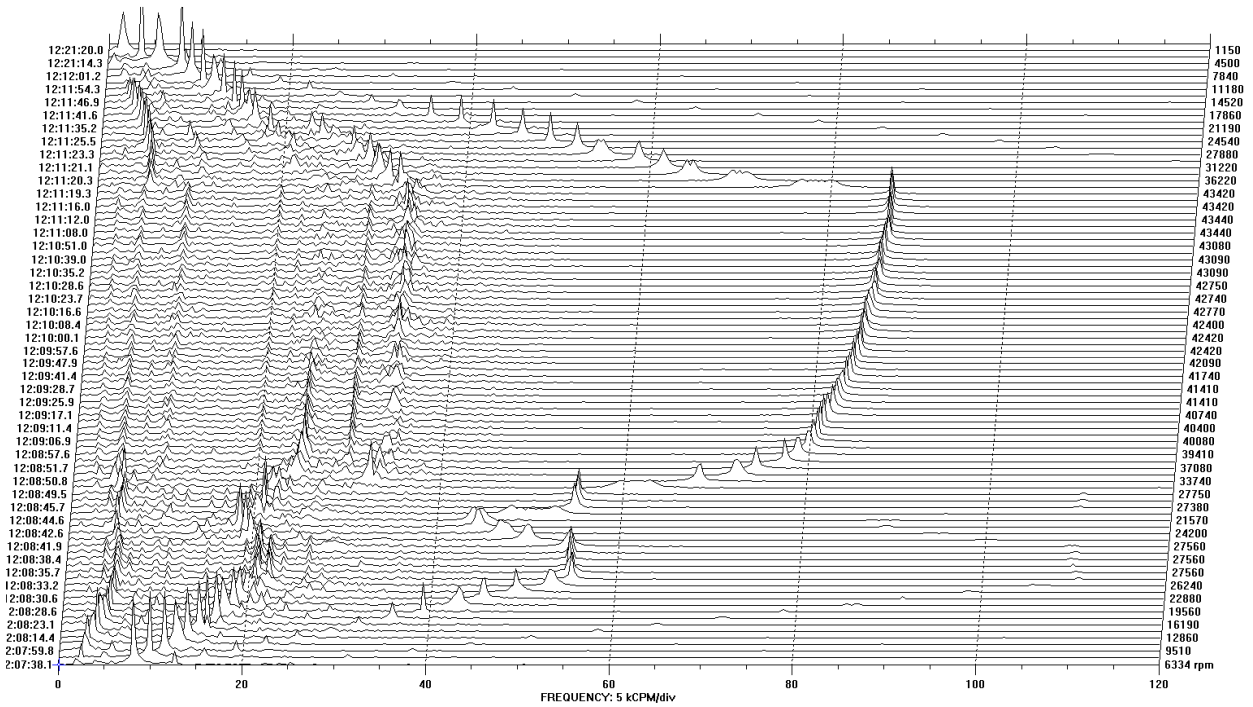

Figure A.18 Run 35, Uc=0, Ut=0.342 g-mm, Nmax= 89600 RPM

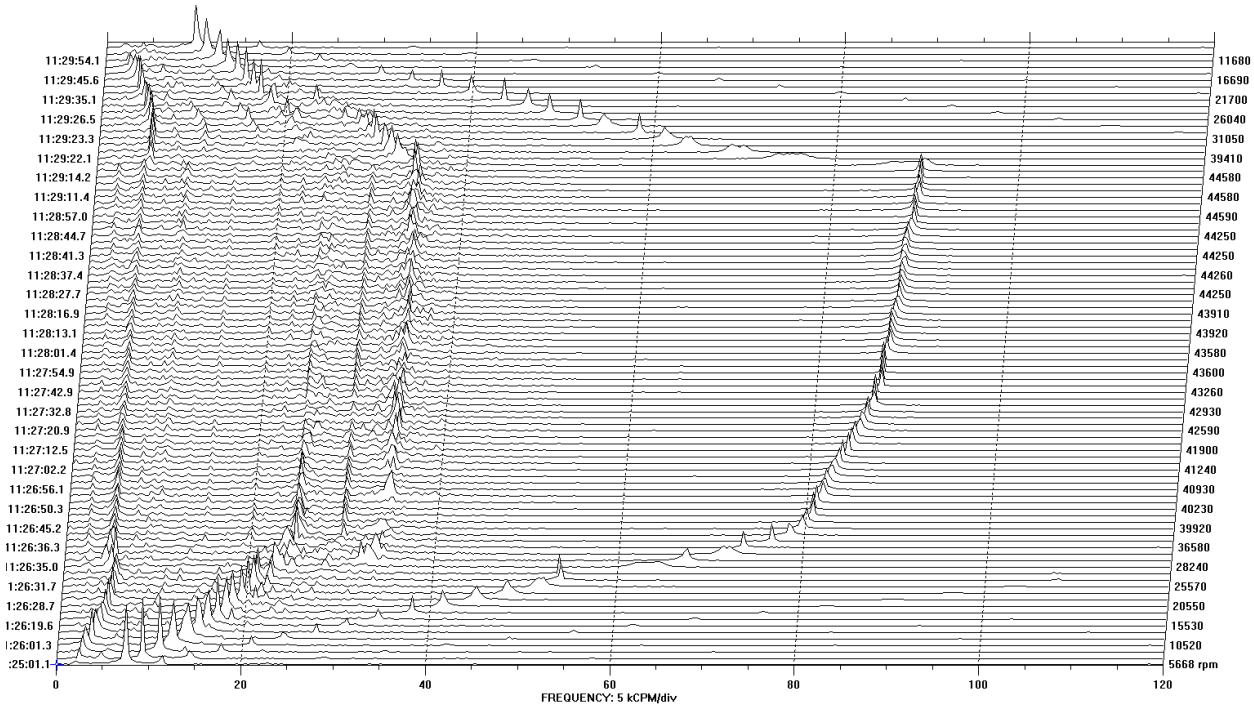

Figure A.19 Run 36, Uc=0, Ut=0.342 g-mm, Nmax=86840 RPM

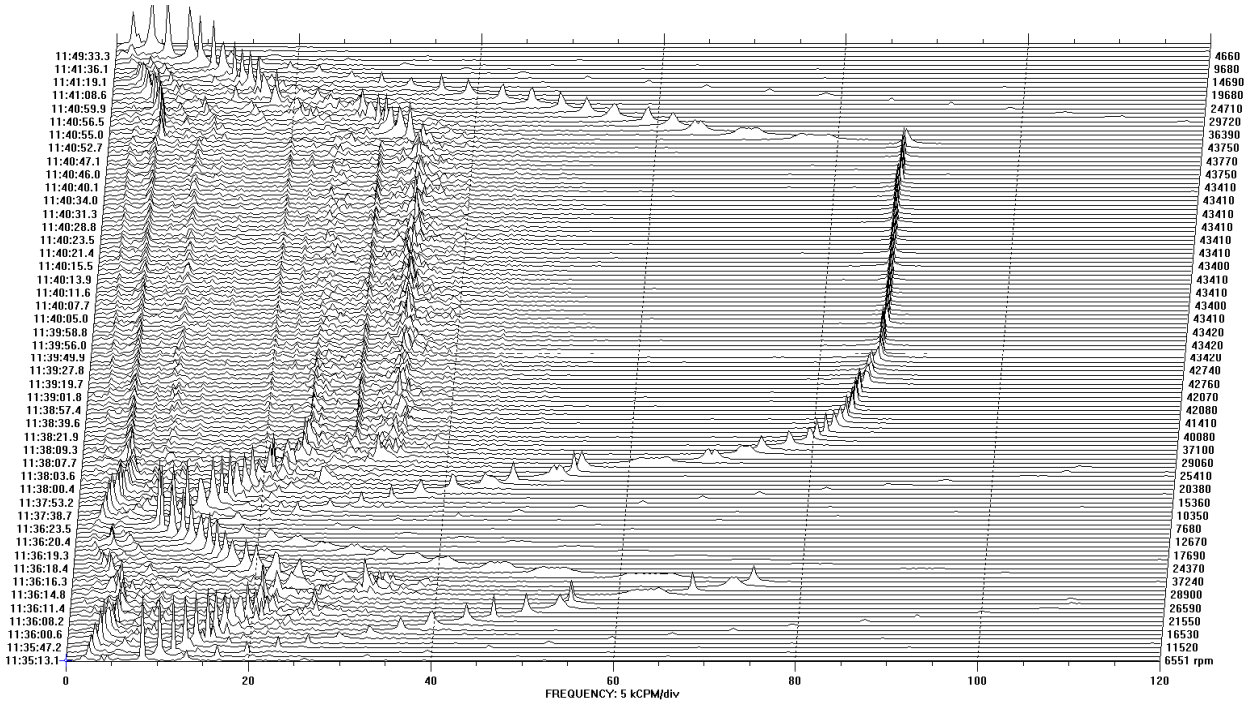

Figure A.20 Run 37, Uc=0, Ut=0.342, Nmax=87540 RPM

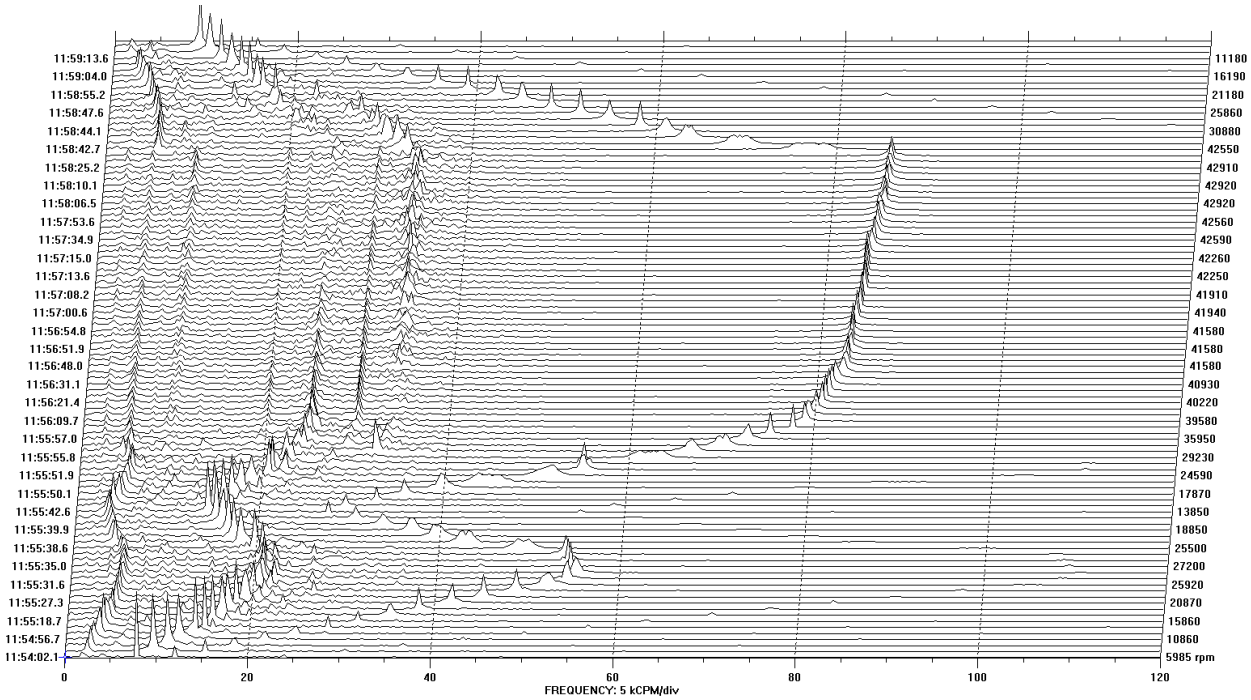

Figure A.21 Run 38, Uc=0.302 g-mm, Ut=0.342 g-mm, Nmax= 85840

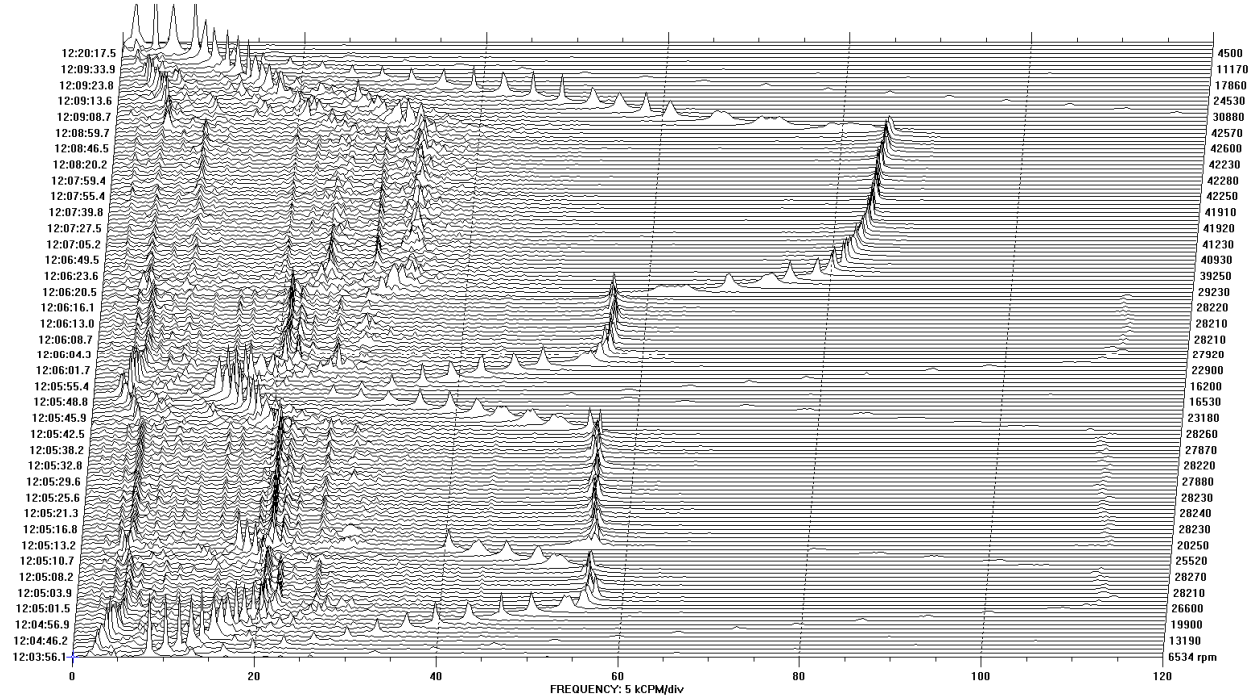

Figure A.22 Run 39, Uc=0.302 g0mm, Ut=0.342 g-mm, Nmax=85200 RPM

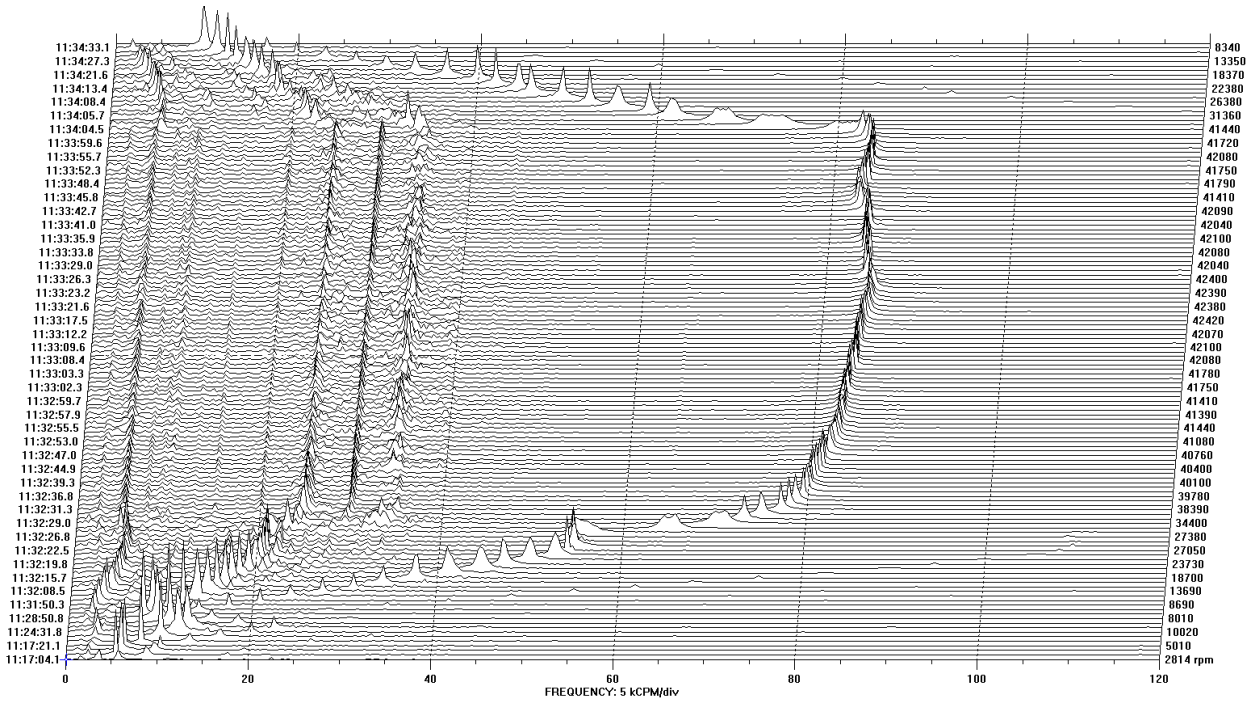

Figure A.23 Run 40, Uc=0.906 g-mm, Ut=0.342 g-mm, Nmax= 84800 RPM

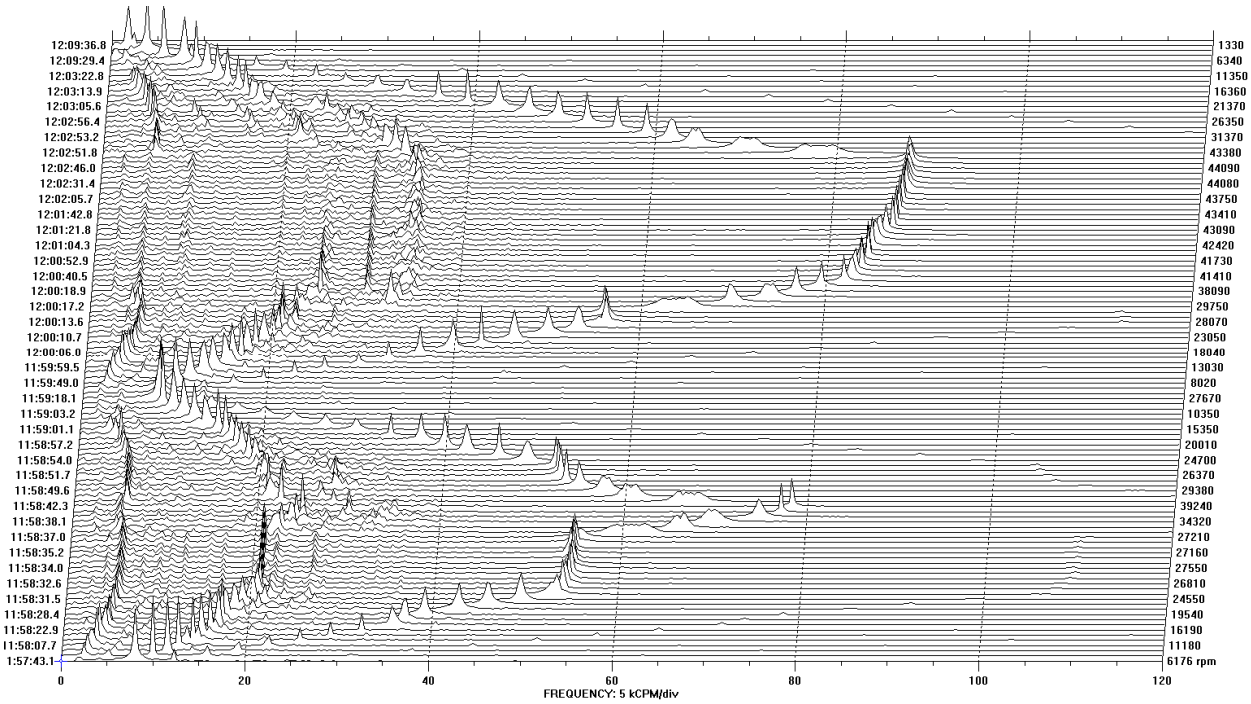

Figure A.24 Run 43, Uc= 0.604 g-mm, Ut=0.342 g-mm, Nmax= 88180 RPM

APPENDIX B

Wheel Prints

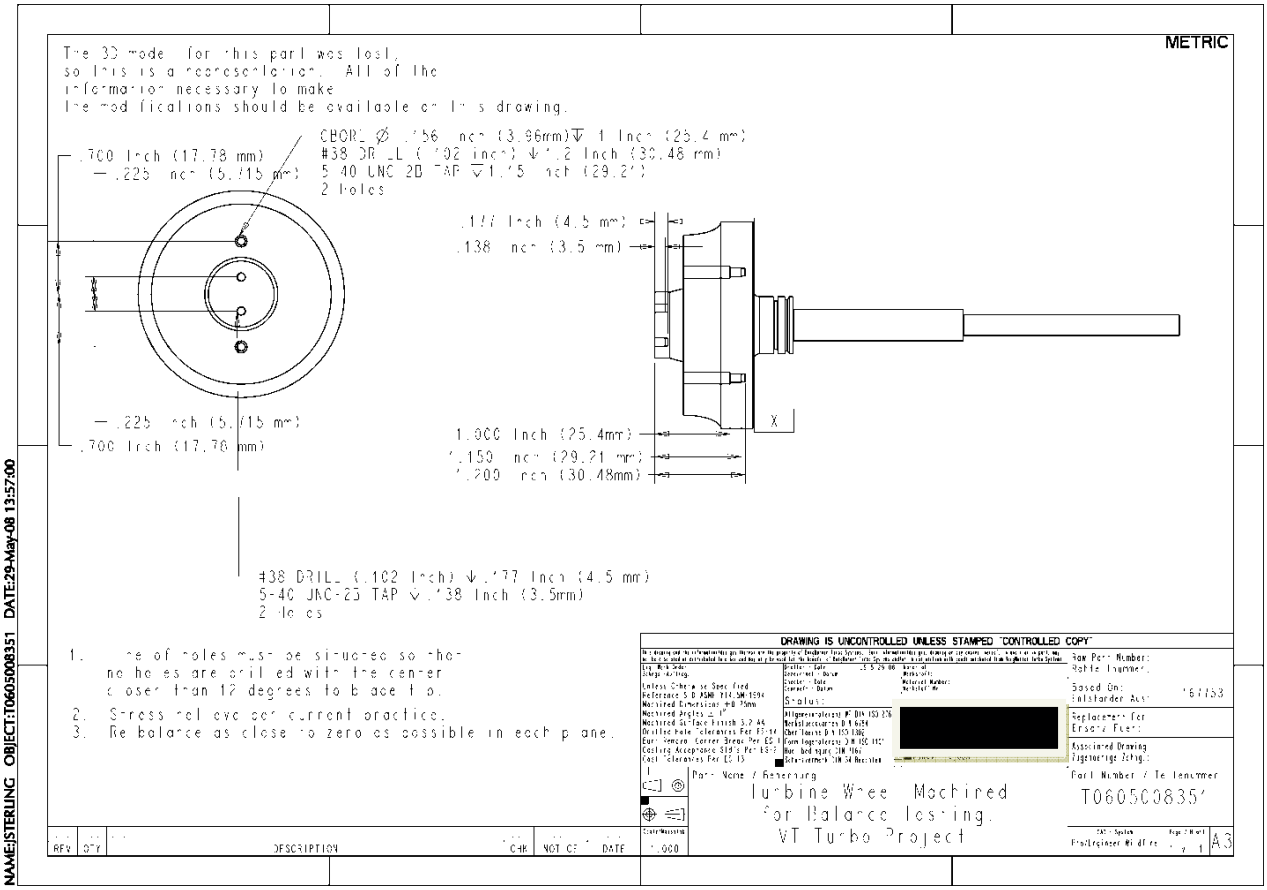

Figure B.1 Turbine Wheel Print

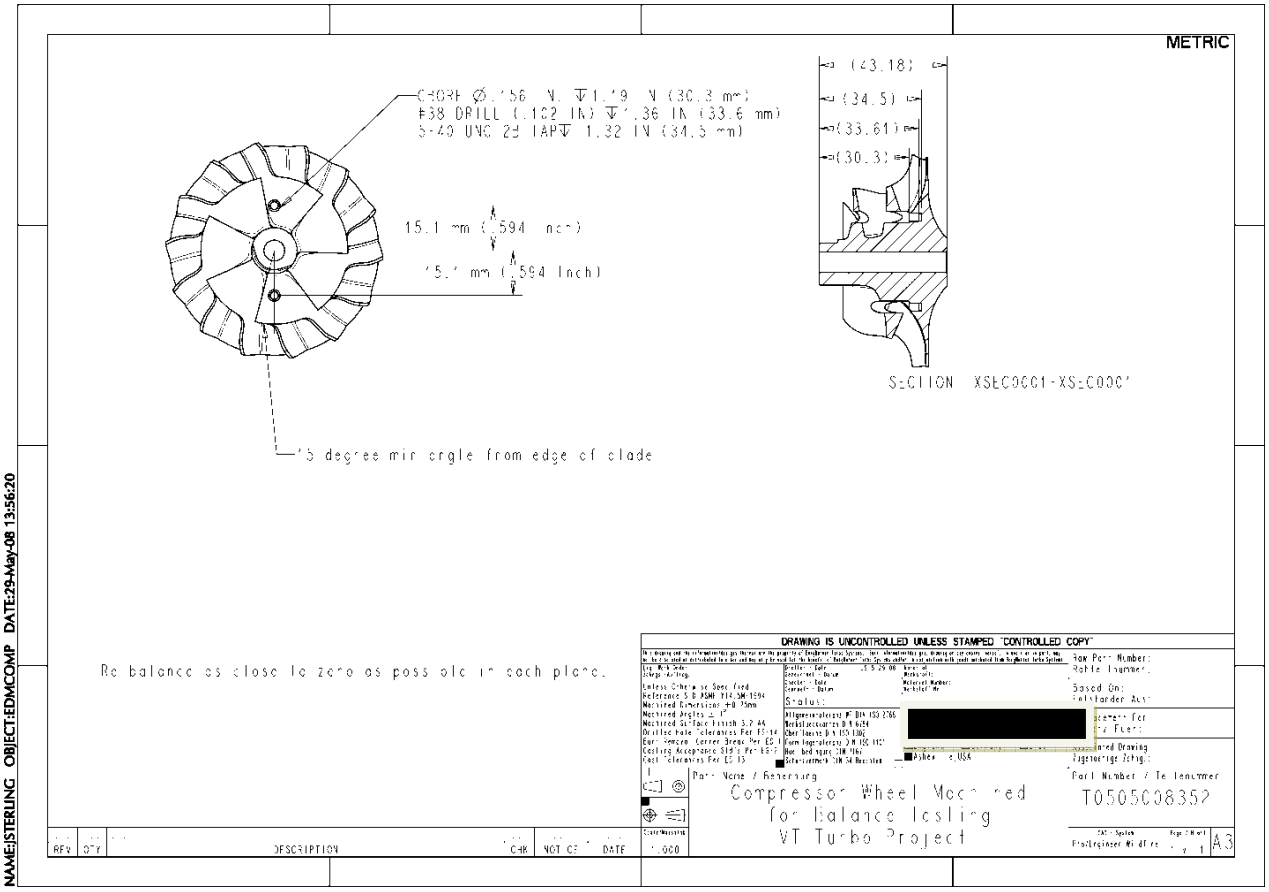

Figure B.2 Compressor Wheel Print